2021-06

MASS FLOW MEASUREMENT IN THE INLET OF A TRANSONIC AXIAL COMPRESSOR

Grant, Travis M.

Monterey, CA; Naval Postgraduate School

NAVAL POSTGRADUATE SCHOOL

MONTEREY, CALIFORNIA

THESIS

MASS FLOW MEASUREMENT IN THE INLET OF A TRANSONIC AXIAL COMPRESSOR

by

Travis M. Grant

June 2021

Thesis Advisor:	Walter Smith
Co-Advisor:	Anthony J. Gannon
Second Reader:	Garth V. Hobson

THIS PAGE INTENTIONALLY LEFT BLANK

REPORT DOCUMENTATION PAGE			*Form Approved OMB No. 0704-0188*

1. AGENCY USE ONLY *(Leave blank)*	**2. REPORT DATE** June 2021	**3. REPORT TYPE AND DATES COVERED** Master's thesis

4. TITLE AND SUBTITLE MASS FLOW MEASUREMENT IN THE INLET OF A TRANSONIC AXIAL COMPRESSOR	**5. FUNDING NUMBERS** RMNP6
6. AUTHOR(S) Travis M. Grant	
7. PERFORMING ORGANIZATION NAME(S) AND ADDRESS(ES) Naval Postgraduate School Monterey, CA 93943-5000	**8. PERFORMING ORGANIZATION REPORT NUMBER**
9. SPONSORING / MONITORING AGENCY NAME(S) AND ADDRESS(ES) ONR, Arlington, VA 22217	**10. SPONSORING / MONITORING AGENCY REPORT NUMBER**

11. SUPPLEMENTARY NOTES The views expressed in this thesis are those of the author and do not reflect the official policy or position of the Department of Defense or the U.S. Government.

12a. DISTRIBUTION / AVAILABILITY STATEMENT Approved for public release. Distribution is unlimited.	**12b. DISTRIBUTION CODE** A

13. ABSTRACT (maximum 200 words)

This study sought to determine the discharge coefficient of the inlet bell mouth of a transonic compressor rig both experimentally and through computational fluid dynamics. The new inlet bell mouth was integrated into the test rig to provide more favorable flow conditions for more accurate measurement of the mass flow rate entering the rig. A computational fluid dynamics analysis was conducted using a 3-D model of the inlet of the test rig to obtain a preliminary prediction of the flow profile in the bell mouth. This analysis drove the design of a rake probe of pitot tubes that was mounted in the exit plane of the bell mouth to measure the actual flow profile. This allowed for the calculation of the actual mass flow rate, which could then be compared to the ideal mass flow rate to produce a discharge coefficient. This discharge coefficient can be used in future testing as a method of calculating the actual mass flow rate from only the measured ideal mass flow rate.

14. SUBJECT TERMS transonic rotor, transonic compressor, mass flow rate measurement, computational fluid dynamics, CFD, axial compressor, bell mouth, rake probe	**15. NUMBER OF PAGES** 91
	16. PRICE CODE

17. SECURITY CLASSIFICATION OF REPORT	**18. SECURITY CLASSIFICATION OF THIS PAGE**	**19. SECURITY CLASSIFICATION OF ABSTRACT**	**20. LIMITATION OF ABSTRACT**
Unclassified	Unclassified	Unclassified	UU

NSN 7540-01-280-5500

Standard Form 298 (Rev. 2-89)
Prescribed by ANSI Std. 239-18

THIS PAGE INTENTIONALLY LEFT BLANK

Approved for public release. Distribution is unlimited.

MASS FLOW MEASUREMENT IN THE INLET OF A TRANSONIC AXIAL COMPRESSOR

Travis M. Grant
Ensign, United States Navy
BS, United States Naval Academy, 2020

Submitted in partial fulfillment of the
requirements for the degree of

**MASTER OF SCIENCE IN ENGINEERING SCIENCE
(AEROSPACE ENGINEERING)**

from the

**NAVAL POSTGRADUATE SCHOOL
June 2021**

Approved by: Walter Smith
Advisor

Anthony J. Gannon
Co-Advisor

Garth V. Hobson
Second Reader

Garth V. Hobson
Chair, Department of Mechanical and Aerospace Engineering

THIS PAGE INTENTIONALLY LEFT BLANK

ABSTRACT

This study sought to determine the discharge coefficient of the inlet bell mouth of a transonic compressor rig both experimentally and through computational fluid dynamics. The new inlet bell mouth was integrated into the test rig to provide more favorable flow conditions for more accurate measurement of the mass flow rate entering the rig. A computational fluid dynamics analysis was conducted using a 3-D model of the inlet of the test rig to obtain a preliminary prediction of the flow profile in the bell mouth. This analysis drove the design of a rake probe of pitot tubes that was mounted in the exit plane of the bell mouth to measure the actual flow profile. This allowed for the calculation of the actual mass flow rate, which could then be compared to the ideal mass flow rate to produce a discharge coefficient. This discharge coefficient can be used in future testing as a method of calculating the actual mass flow rate from only the measured ideal mass flow rate.

THIS PAGE INTENTIONALLY LEFT BLANK

TABLE OF CONTENTS

LIST OF FIGURES

THIS PAGE INTENTIONALLY LEFT BLANK

LIST OF TABLES

THIS PAGE INTENTIONALLY LEFT BLANK

LIST OF ACRONYMS AND ABBREVIATIONS

CFD	computational fluid dynamics
NASA	National Aeronautics and Space Administration
NPS	Naval Postgraduate School
NPSMF	Naval Postgraduate School military fan
TCR	transonic compressor rig
TPL	turbo propulsion lab

NOMENCLATURE

C_D	discharge coefficient
C_P	isobaric specific heat
$\dot{m}_{ideal}$	ideal mass flow rate
$\dot{m}_{real}$	real mass flow rate
P_S	static pressure
P_t	total or stagnation pressure
T_t	total or stagnation temperature
v	velocity
γ	ratio of specific heats
μ	dynamic viscosity
ρ	density

ACKNOWLEDGMENTS

I would like to acknowledge the help that Dr. Smith, Dr. Gannon, and Dr. Hobson provided me with throughout the whole process of writing this thesis. They collectively spent many hours talking through design ideas, explaining the complex data acquisition system, helping make my MATLAB scripts better, and many other things. Their guidance was extremely valuable at every step of the way. I would also like to thank John Gibson for his extensive help with manufacturing many parts of my thesis and the wisdom he provided during many of those processes.

THIS PAGE INTENTIONALLY LEFT BLANK

I. INTRODUCTION

A. MOTIVATION

The Turbopropulsion Laboratory (TPL) at Naval Postgraduate School (NPS) is conducting on-going testing of transonic axial compressor fans. The Transonic Compressor Rig (TCR) at the TPL is currently dedicated to the testing of the NPS Military Fan (NPSMF), a transonic axial compressor rotor. The testing of the NPSMF analyzes a variety of performance characteristics for the NPSMF, particularly the conditions when the compressor stalls.

The analysis of stall characteristics requires a very precise measurement of the mass flow rate through the TCR. The methods used to collect mass flow rate data in the TCR in the past have been non-optimal. A new inlet bell mouth has been designed to produce more ideal flow conditions which provides an opportunity for more precise measurements of mass flow rate. Providing a means of obtaining highly accurate mass flow rate data will benefit all future work in the TCR and aid in compressor stall prediction. Research concerning compressor stall is of particular importance to the Navy because compressor stall presents a serious hazard to aircraft conducting carrier flight operations.

B. LITERATURE REVIEW

Mass flow measurements through bell mouths in turbomachinery applications have been taken by means of rake probes for decades. Research conducted by Smith [1] and sponsored by the National Aeronautics and Space Administration (NASA) in 1985 utilized a bell mouth for mass flow rate measurements. The research involved installing a rake probe in the throat of the bell mouth from which to calculate the actual mass flow rate and calibrate the bell mouth. The result of the study was the discharge coefficient of the bell mouth, which was found to range from 0.966 to 0.972. Smith [1] determined that the discharge coefficient of the bell mouth was not significantly influenced by the Reynolds number.

Elliptical profile bell mouth flow meters are known to have discharge coefficients very close to unity, making them advantageous for use in mass flow measurements [2].

Additionally, discharge coefficients close to unity are less subject to measurement uncertainty [2]. Research by Ito, Watanabe, and Shoji determined the discharge coefficient of a long-radius inlet nozzle to vary between approximately 0.88 and 0.99 over a wide range of Reynold's numbers (spanning two orders of magnitude) [3]. The data from Ito, Watanabe, and Shoji are shown in Figure 1.

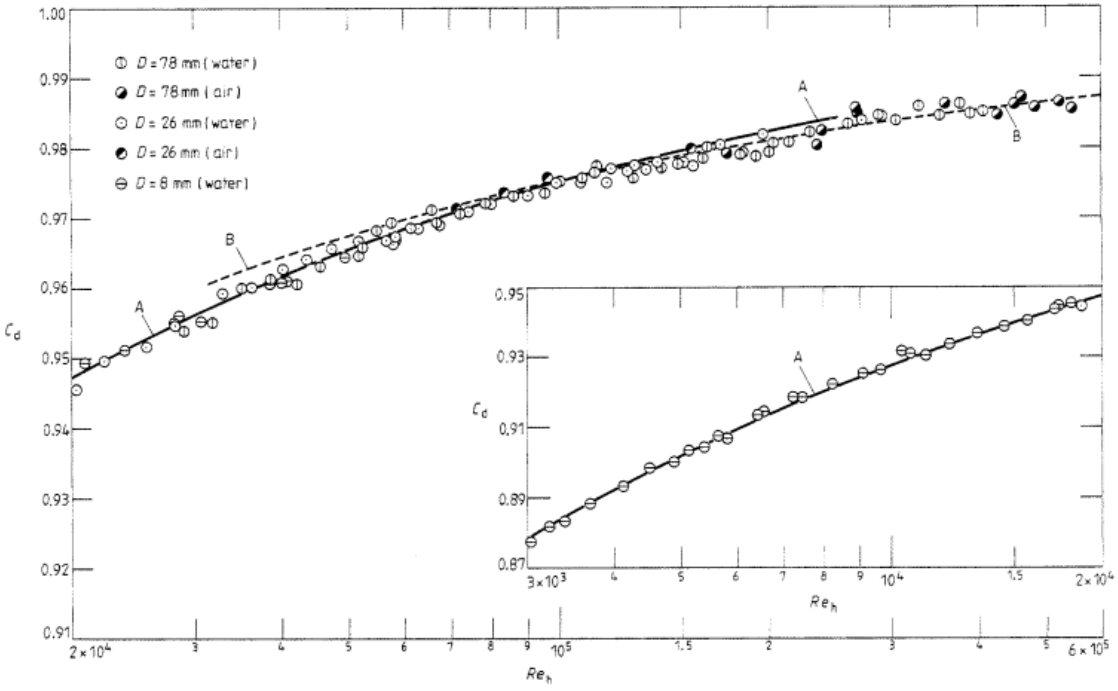

Figure 1. Discharge coefficient as a function of Reynold's number by Ito, Watanabe, and Shoji. Source: [3].

C. THESIS OBJECTIVES

The overall objective of this study was to attain an accurate means of measuring mass flow rate through the inlet of the TCR. To achieve this, a new bell mouth inlet will be implemented that provides better flow conditions for the mass flow rate measurements as compared to the previous methods used in the TCR. Computational Fluid Dynamics (CFD) will be used to generate a working simulation that accurately models the flow entering the TCR. This simulation will be used as a scoping tool and will drive the design of a rake probe that will serve as a means of measuring mass flow rate and calibrating the new bell mouth inlet.

II. BACKGROUND INFORMATION

A. PREVIOUS WORK

The bell mouth inlet was designed by Wallen [4] to be attached to the inlet of the TCR. An elliptical profile at the leading edge was determined to be the most efficient [4] and an example of this elliptical profile is shown in Figure 2. The bell mouth was designed with an exit throat diameter of 0.3048 meters and elliptical radii of 0.3048 meters and 0.1016 meters, respectively.

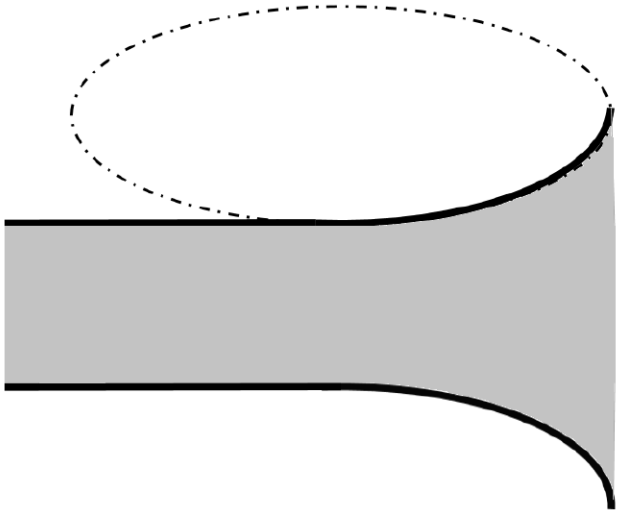

Figure 2. Elliptical profile bell mouth as described by Wallen. Source: [4].

The bell mouth was to be made of 6061 Aluminum and type III hard coat anodized. The bell mouth will be outside exposed to the elements, so the anodizing will prevent oxidation of the surface over time. It was designed to be constructed of four sections that were to be bolted together in an effort to make manufacturing simpler [4]. The model of the bell mouth is shown in Figure 3.

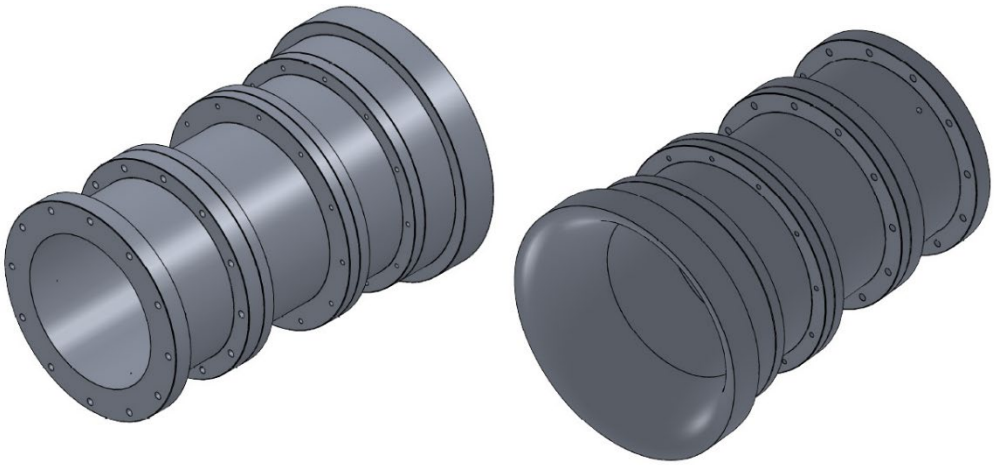

Figure 3. Bell mouth inlet as designed by Wallen (left), rear view (right), and front view. Source: [4].

The bell mouth was designed to attach to the inlet of the TCR via a large diameter casing that surrounds the throttle of the TCR. The purpose of the casing is to provide an airtight plenum around the throttle so that air coming through the bell mouth inlet would not be restricted further before entering the throttle and no outside influences could affect the air after passing through the bell mouth and before entering the throttle. The throttle surrounded by the throttle casing on the TCR is shown in Figure 4.

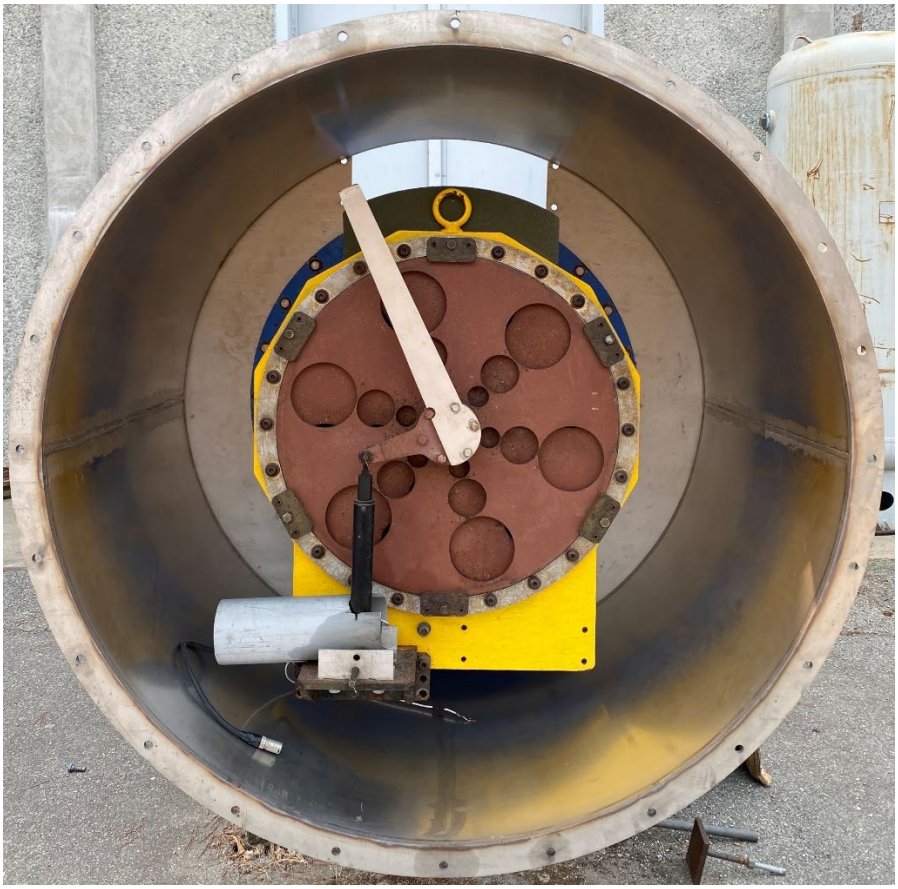

Figure 4. Throttle surrounded by the throttle casing, to which the bell mouth would be attached.

The smaller diameter bell mouth and the larger diameter throttle casing are connected by a cone attachment. The assembly of the bell mouth, cone attachment, and throttle casing is shown in Figure 5.

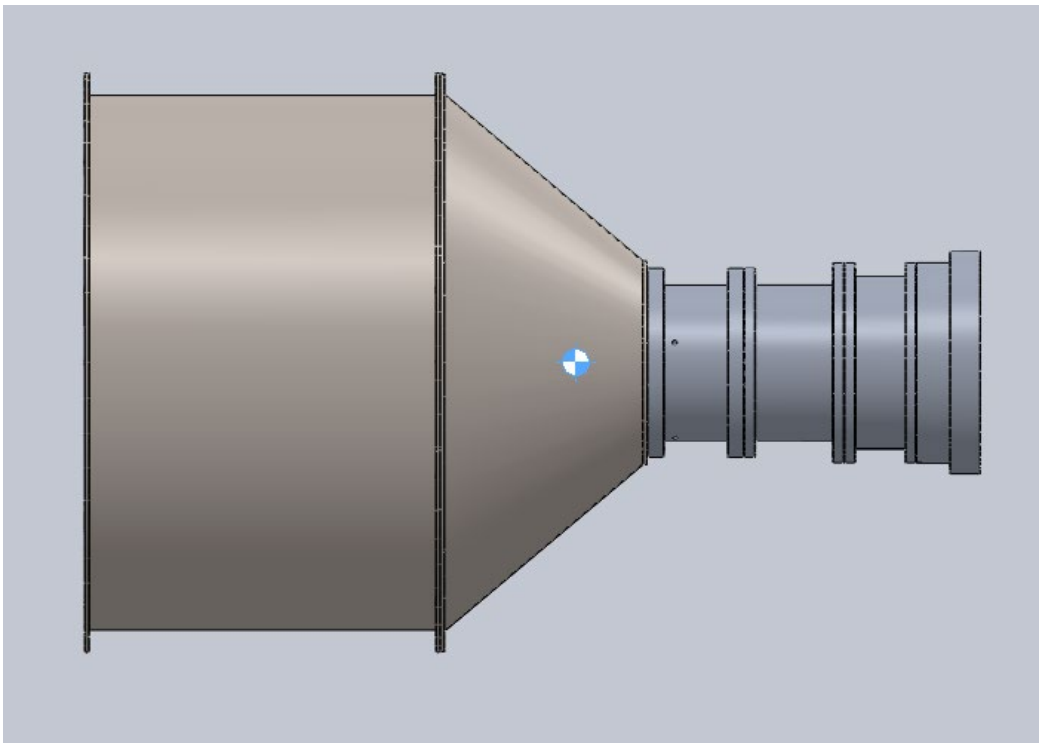

Figure 5. Assembly of throttle casing, cone attachment and bell mouth as designed by Wallen. Source: [4].

B. MASS FLOW MEASUREMENTS

In many turbomachinery applications, mass flow rates are obtained through flow restriction type devices such as orifices, venturis, and bell mouths. These devices operate by pulling air through them bringing the flow to some velocity which will be calculated through the difference in pressure in the device and upstream of the device. An example of a bell mouth is shown in Figure 6. A pressure port in the throat of the bell mouth measures static pressure and a pressure port upstream of the bell mouth where velocity is nearly zero measures the total pressure.

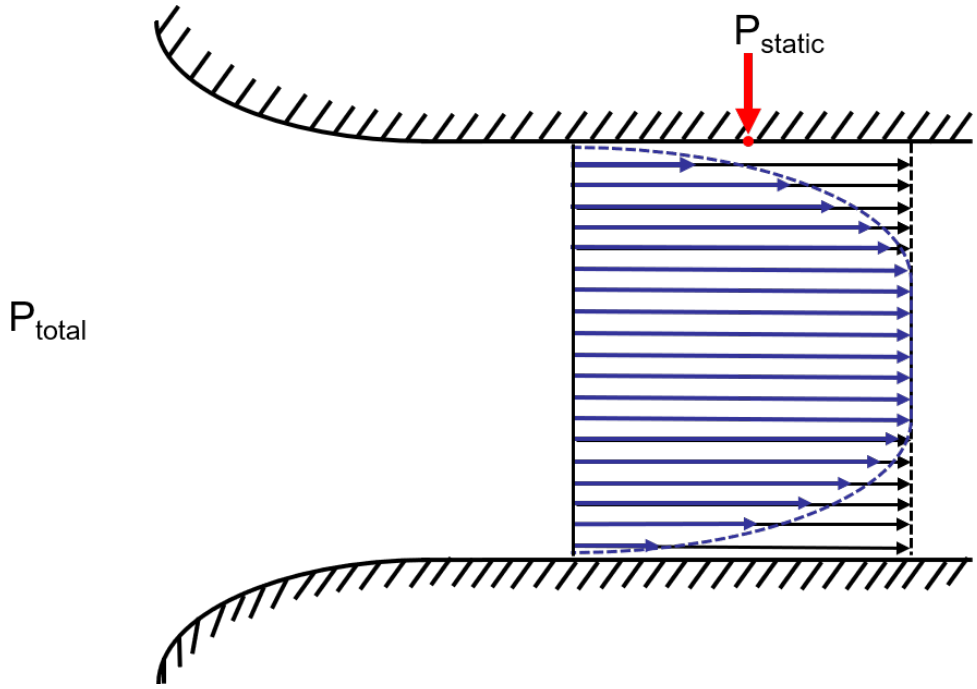

Figure 6. Representation of the difference between the real and ideal mass flow rate in a bell mouth.

The flow into the bell mouth can be approximated using a uniform velocity profile, shown by the black arrows in Figure 6. In reality, the flow cannot have this uniform profile. Friction losses take place at the wall of the bell mouth and create a developing boundary layer along the wall. The flow through the bell mouth will follow a profile similar to the one shown by the blue arrows in Figure 6. The actual shape of the profile is not known and it is also not perfectly constant. The real mass flow rate through the bell mouth requires the average of the flow profile to be measured accurately to take into account the boundary layer. To measure the profile, a CFD analysis will be used to obtain an approximation of the profile as a scoping tool. This approximation will then govern the design of a rake probe to be mounted in the throat of the bell mouth to measure the real flow profile.

The rake probe is intended to calibrate the bell mouth and then be removed. The goal of knowing the velocity profile is obtaining the discharge coefficient. The discharge coefficient is the ratio of real mass flow rate to ideal mass flow rate and is shown in Equation 1.

$$C_D = \frac{\dot{m}_{real}}{\dot{m}_{ideal}} \tag{1}$$

The discharge coefficient allows invasive measurement devices such as the rake probe, which create disturbances in the flow, to be removed. The real mass flow rate can then be obtained by calculating the ideal mass flow rate based on the measured static pressures and total pressure and then correcting that ideal mass flow rate using the discharge coefficient.

The actual measurements taken in the bell mouth are pressures. These pressures must be related to velocities in order to calculate mass flow rate. The flow has too high of a Mach number to be treated as incompressible. To calculate the velocity of the compressible flow, a simplified version of the energy equation and isentropic flow relationships are required. The simplified version of the energy equation is shown in Equation 2.

$$C_P T_t = \frac{1}{2} v_o^2 \tag{2}$$

In this version of the energy equation, v_o is the maximum velocity a flow could achieve if all the thermal energy in the flow where it has zero velocity was converted to kinetic energy. Additionally, C_P is the isobaric specific heat of the fluid and T_t is the total temperature. This maximum velocity is adjusted via isentropic flow relationships to calculate what fraction of the maximum velocity is actually achieved by the flow based on the ratio between the static and total pressures. These combine into Equation 3

$$v = \sqrt{2C_P T_t}\sqrt{1-(\frac{P_S}{P_t})^{\frac{\gamma-1}{\gamma}}}\ , \tag{3}$$

where v is the velocity of the flow, P_S is the static pressure, and P_t is the total pressure, and γ is the ratio of specific heats.

Equation 3 will calculate the average velocity of the flow across the bell mouth or the local velocity at a given point in the flow, depending on which total pressure is used in the calculation. For the average velocity across the entire bell mouth, the total pressure

measured upstream of the bell mouth where velocity is close to zero is used. This is how the uniform velocity profile from Figure 6 and the ideal mass flow rate are obtained. The local velocity at a discrete location in the flow is obtained by using the stagnation pressure at that discrete location, which is collected by a pitot tube on the rake probe. The velocity at many discrete locations in the flow can then be integrated over the cross section of the bell mouth to determine the real mass flow rate.

THIS PAGE INTENTIONALLY LEFT BLANK

III. COMPUTATIONAL FLUID DYNAMICS

A CFD analysis using ANSYS CFX is the first step towards measuring the real velocity profile and real mass flow rate through the bell mouth. The CFD analysis provides an approximation of the flow at the exact location in the bell mouth where mass flow rate is to be measured. The primary data desired from the analysis are axial velocities along a radial line in throat of the bell mouth at the location where physical measurements are to be taken. Additionally, the mass flow rate as computed by ANSYS, the static pressure where it is measured in the bell mouth, and the total pressure at ambient conditions are simulated.

A. MODEL GEOMETRY

The geometry used for the CFD analysis is the cross section of the inlet to the TCR from the atmosphere to the throttle. This includes the throttle casing, cone attachment, and bell mouth inlet. The model of these parts, designed by Wallen [4], is shown in Figure 7.

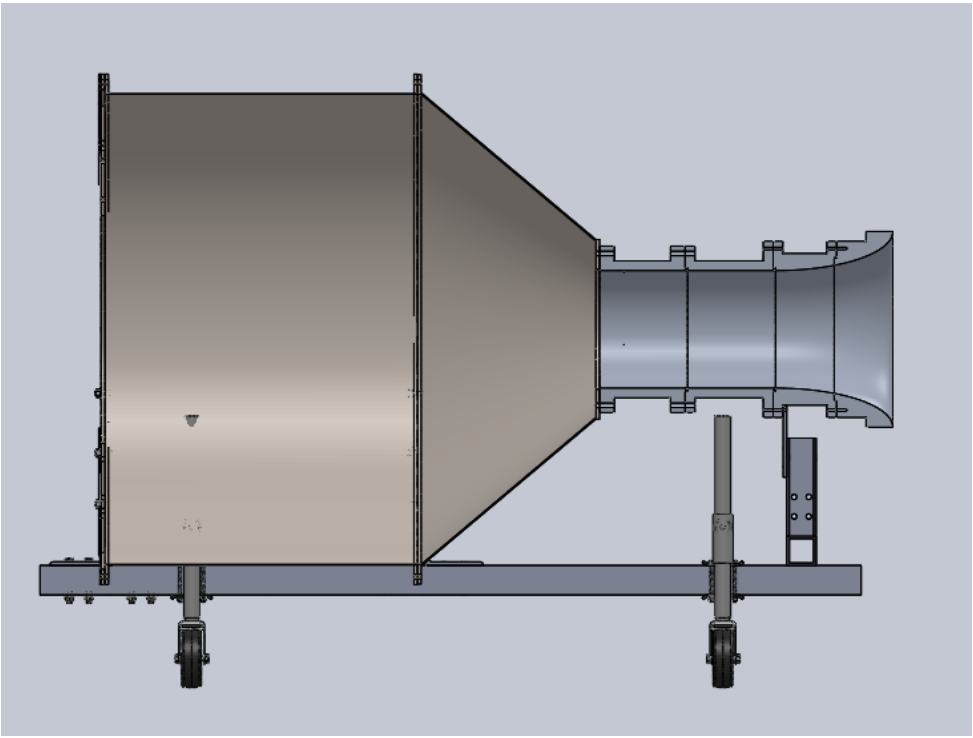

Figure 7. Throttle casing and bell mouth inlet.

The inside contour of the throttle casing, cone attachment, and bell mouth inlet as well as the shape of the throttle that fits inside the throttle casing were used as the boundaries of the flow volume to be put into ANSYS CFX. The model used in CFX overlapped onto the Solidworks model, to show that the models indeed match, is shown in Figures 8 and 9. The model, however, involved several simplifications. The bell mouth inlet is approximately a meter above the ground, but the ground was neglected. The throttle is actuated by a device that is mounted just upstream of the throttle, but it is not included in this model. The four sections of the bell mouth have interfaces with a possible interface tolerance up to 0.0254 millimeters, but the numerical model represents the bell mouth as smooth.

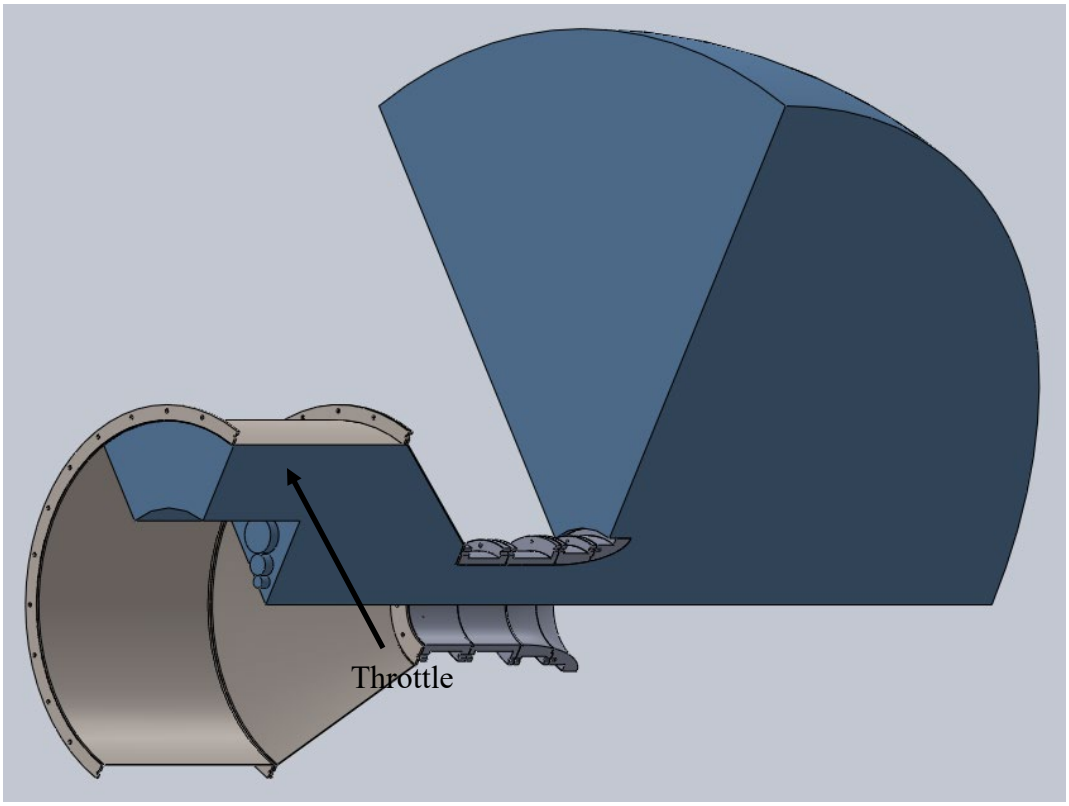

Figure 8. Solidworks model with CFX model overlapped.

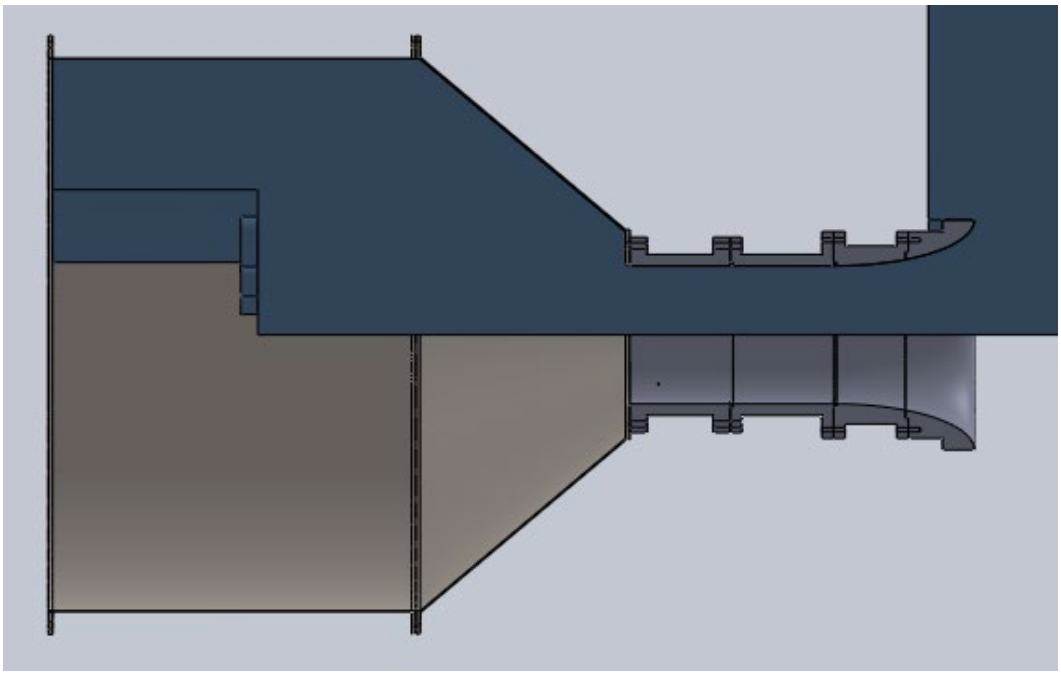

Figure 9. Solidworks model with CFX model overlapped.

The corner where the cone attachment meets the bell mouth is one of the more intricate sections of the geometry. That section is shown in a close-up view in Figure 10 to show that the fluid domain follows the inner wall.

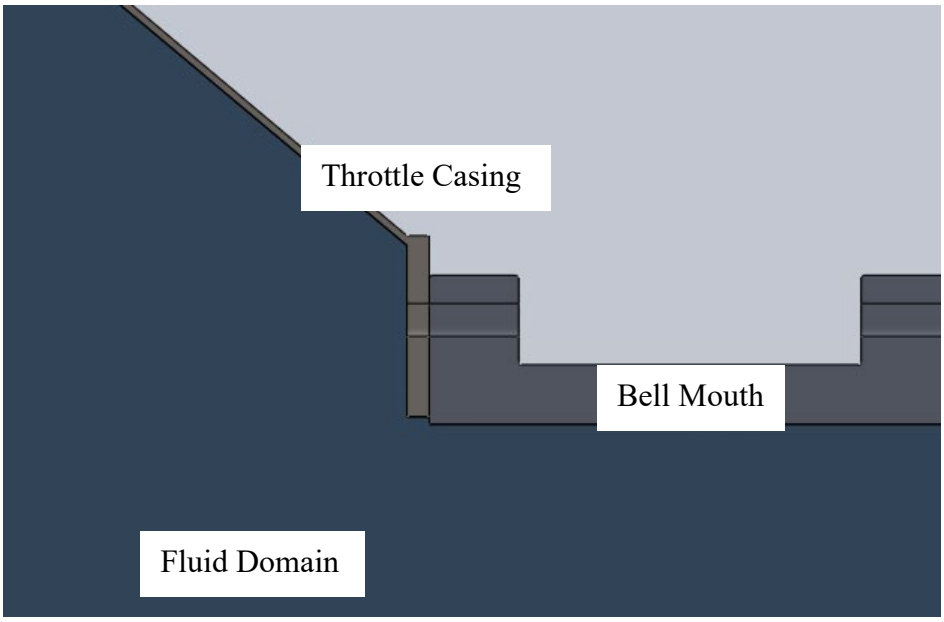

Figure 10. Joint of cone attachment and bell mouth.

The throttle on the TCR consists of six identical columns of three holes each and a plate with the same hole pattern that rotates relative to the throttle to open or close the holes. Therefore, a 60° wedge of the geometry contains one entire column of the holes. With symmetry boundaries on either side of the 60° wedge, this geometry can represent the entire 360° of the TCR. The 60° wedge is shown in Figure 11.

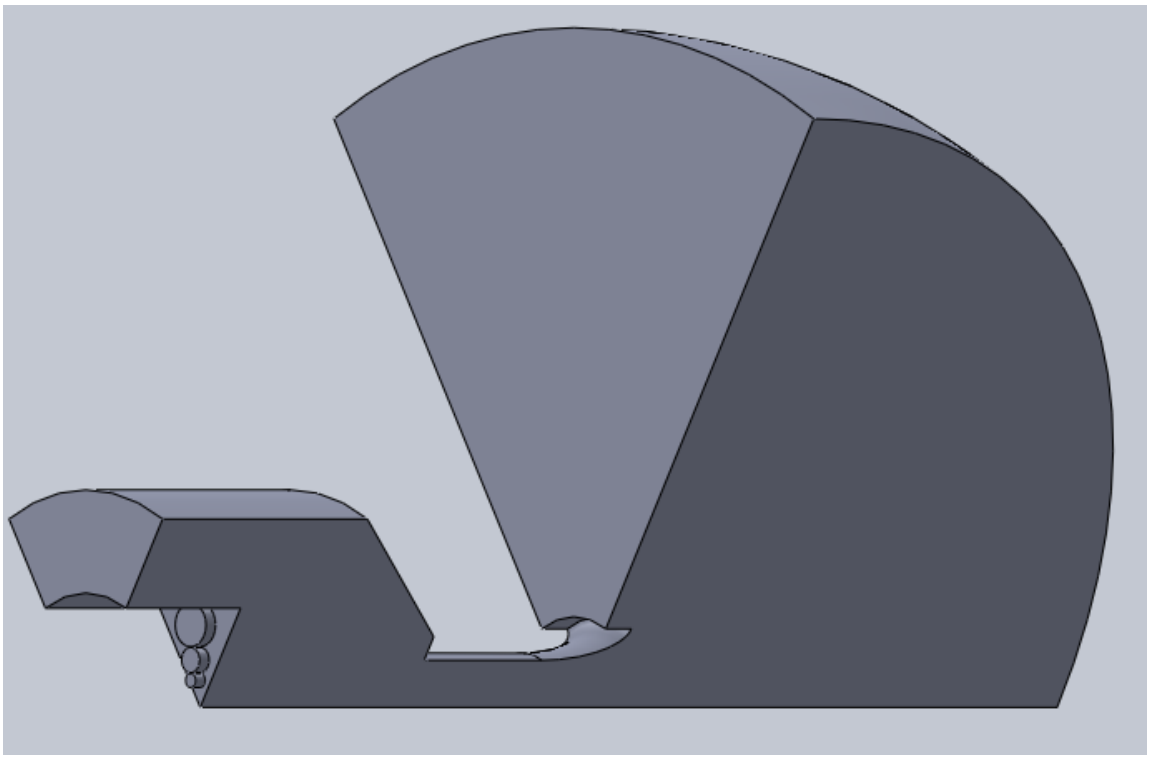

Figure 11. The 60° wedge of the inlet model geometry.

B. ANSYS CFX SETUP

1. Mesh

The geometry includes many sharp corners and complex regions that require the mesh to be refined to properly model the flow in these areas. The bulk global mesh was generated so that maximum element size was 0.02 meters so that the mesh was sufficiently fine in all areas where additional refinement was not needed. Along the walls, 30 inflation layers were added to properly model the boundary layer. The inflation layers in the constant diameter section of the bell mouth would allow pressure measurements at the locations where static ports are located on the actual bell mouth to be more accurate. Additionally, the sizing of the elements around every sharp edge was reduced to significantly refine the mesh close to those sharp edges where the flow could be more complicated. These refinements kept the y+ values to a maximum of 8.542 at the wall, which occurs in the curved section of the bell mouth. Examples of the inflation layers and edge sizing as well as the full mesh are shown in Figures 12–14.

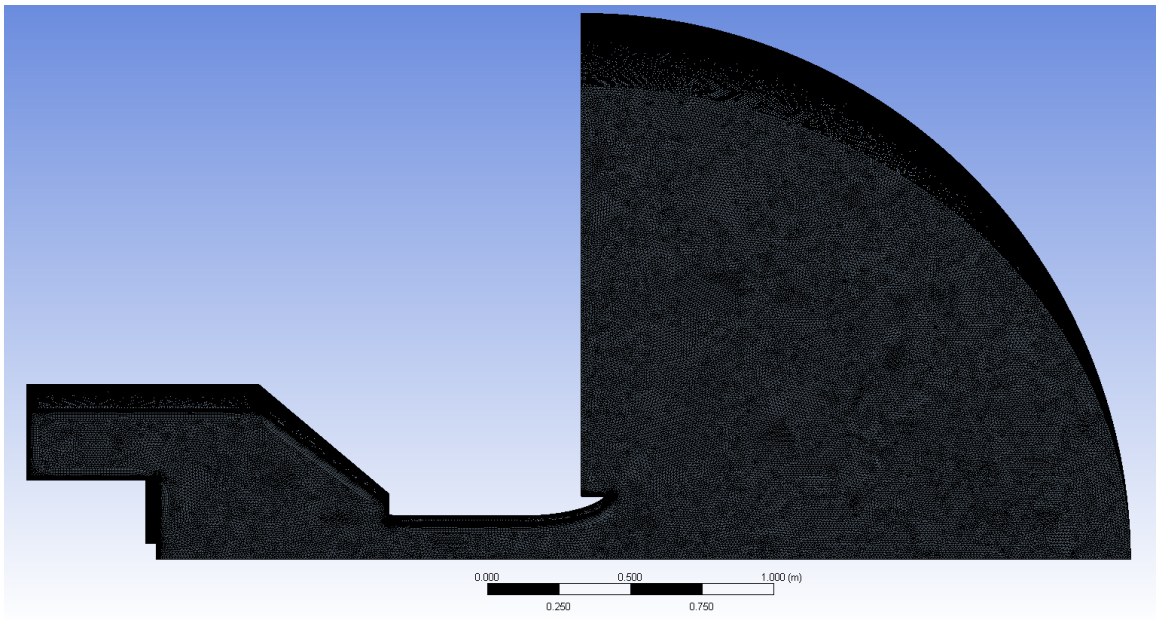

Figure 12. Full mesh of the inlet geometry

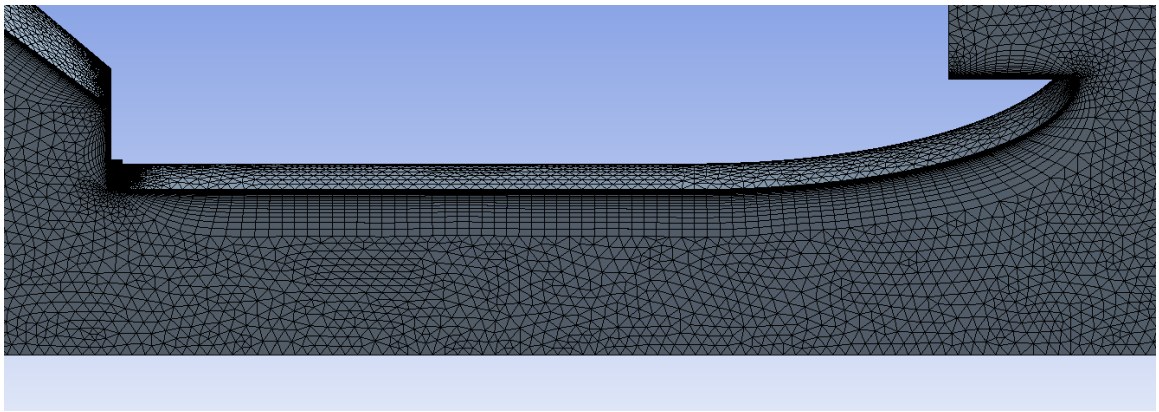

Figure 13. Inflation layers along the wall of the bell mouth

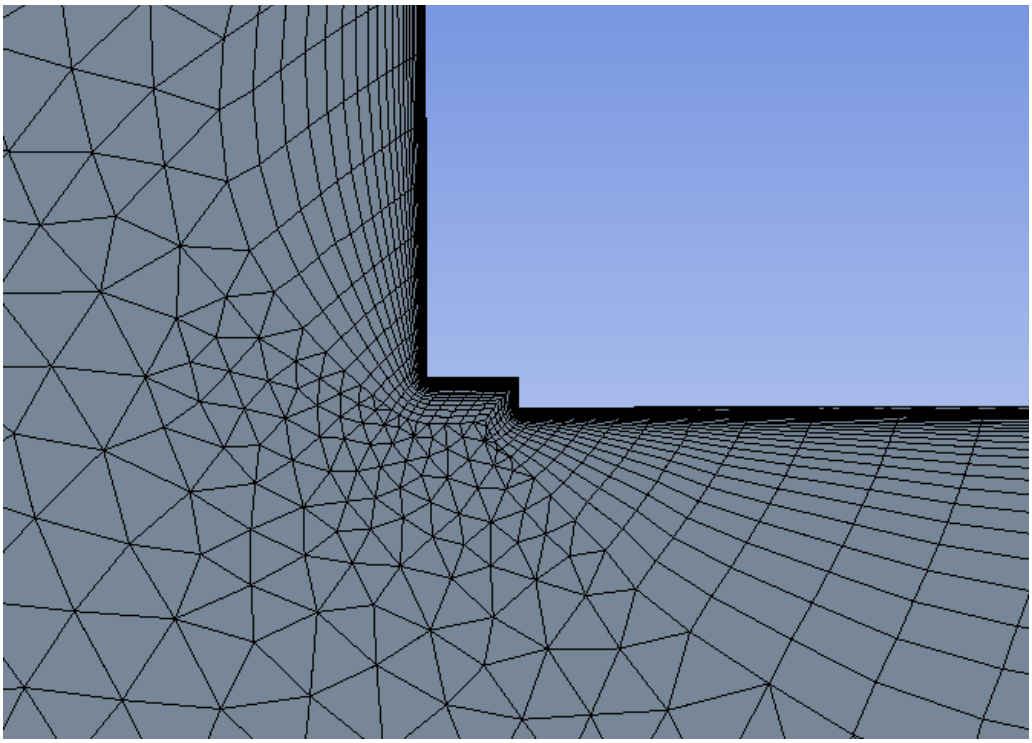

Figure 14. Reduced element size around sharp corners

The statistics of the mesh, including number of elements and number of nodes, are shown in Table 1.

Table 1. Mesh statistics

Number of Elements	9,332,278
Number of Nodes	2,915,882

2. CFX-Pre Setup

The CFX-Pre setup involved setting the fluid properties and boundary conditions properly so that the model would most accurately represent the real flow through the TCR inlet. The material used as the working fluid was set to air ideal gas. The inlet, which in the model is the large curved surface surrounding the bell mouth inlet representing atmospheric air as well as the vertical wall that connects this curved surface to the bell

mouth, was defined as an opening, with the static pressure defined as 0 kPa. This pressure is relative to the reference pressure which was set to 1 standard atmosphere. The outlet, which consists of the 3 throttle holes, was defined as an outlet boundary with an average static pressure of -5 kPa also relative to the 1 atm reference pressure.

The inlet flow should be close to axisymmetric, so the 60° wedge should represent each sixth of the inlet equally. Therefore, the sides of the geometry were defined as symmetry boundaries so that the flow modeled within the geometry would be repeated six times about the center axis of the flow to achieve the entire flow. The walls of the model, which includes the inner surface of the throttle casing, connecting cone, and bell mouth were treated as smooth, adiabatic, no-slip wall. Figure 15 shows the model geometry with the CFX-Pre parameters applied to the respective boundaries.

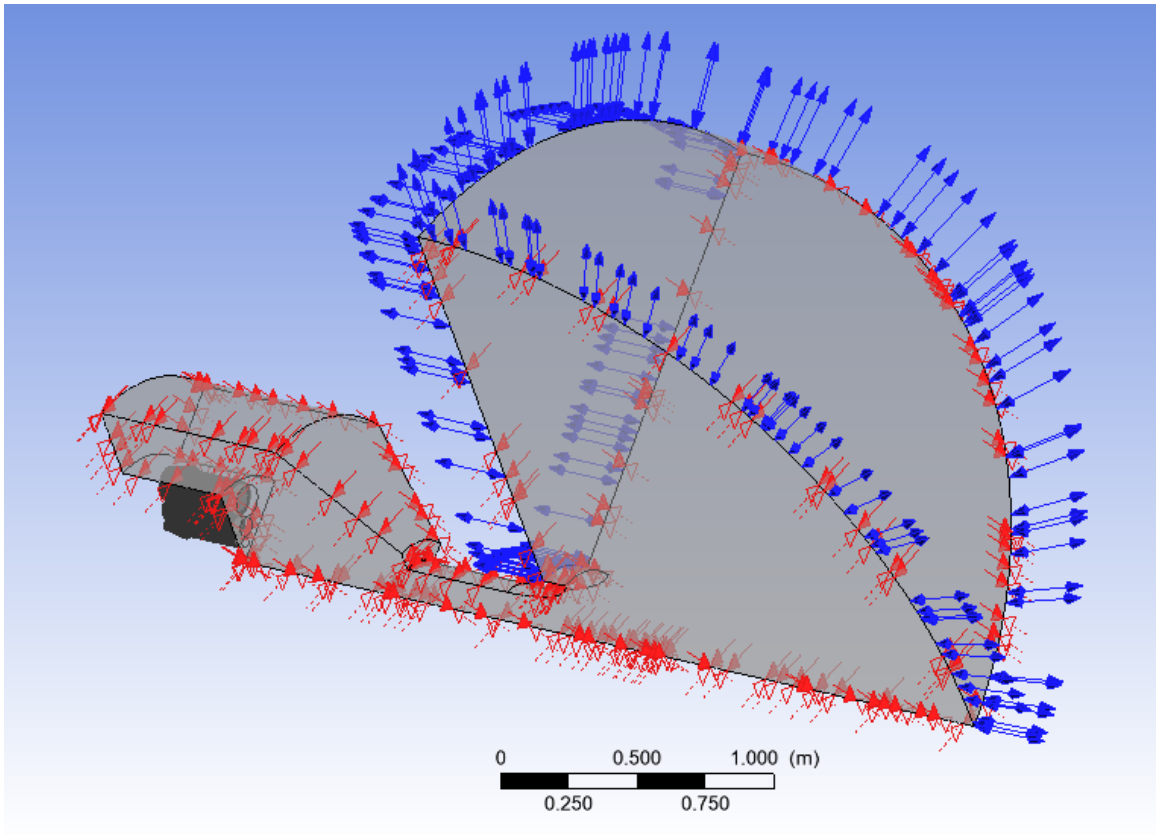

Figure 15. TCR inlet model geometry with boundary conditions applied

3. Mass Flow Expressions

The purpose of the CFD modeling was to calculate the discharge coefficient as a scoping tool to guide the experimental discharge coefficient measurement. Experimentally, complicated instrumentation was implemented to calculate the actual mass flow rate through the bell mouth. Computationally, ANSYS CFX will calculate the mass flow rate through a given portion of the model. The ideal mass flow rate is calculated from the CFD in the same way that it is calculated from the real measurements: by using the static pressure at the wall of the bell mouth and the total pressure which is measured in atmospheric air not influenced by the inlet. This calculated ideal mass flow rate and the actual mass flow rate measured by CFX could be compared to determine the discharge coefficient.

The actual mass flow rate was measured by two separate expressions. The user-defined expression “massin” was defined as the mass flow through the inlet as measured by CFX multiplied by 6, as the 60° wedge is a sixth of the entire TCR inlet. The expression “massout” was defined as the mass flow as measured by CFX through the outlet multiplied by -6 because CFX defines mass flow leaving the system as negative, so the additional negative sign makes the expression positive, allowing easy comparison between the two expressions on a monitor. As the solution converges, the values of “massin” and “massout” approach each other. The converged value of the mass flow is used as the actual mass flow through the model for the discharge coefficient calculation. The monitor of the two mass flow expressions converging is shown in Figure 16 and the expressions as defined in CFX-Pre are shown in Figure 17. The analysis forced the pressures at the inlet and outlet of the model, but did not force a mass flow rate at either. The flow is in the compressible regime, so as the computations are ran, the mass flow entering the system and the mass flow exiting the system are not always the same. The two mass flow rate values converging, along with other convergence criteria, is a good indicator that the analysis has reached steady state.

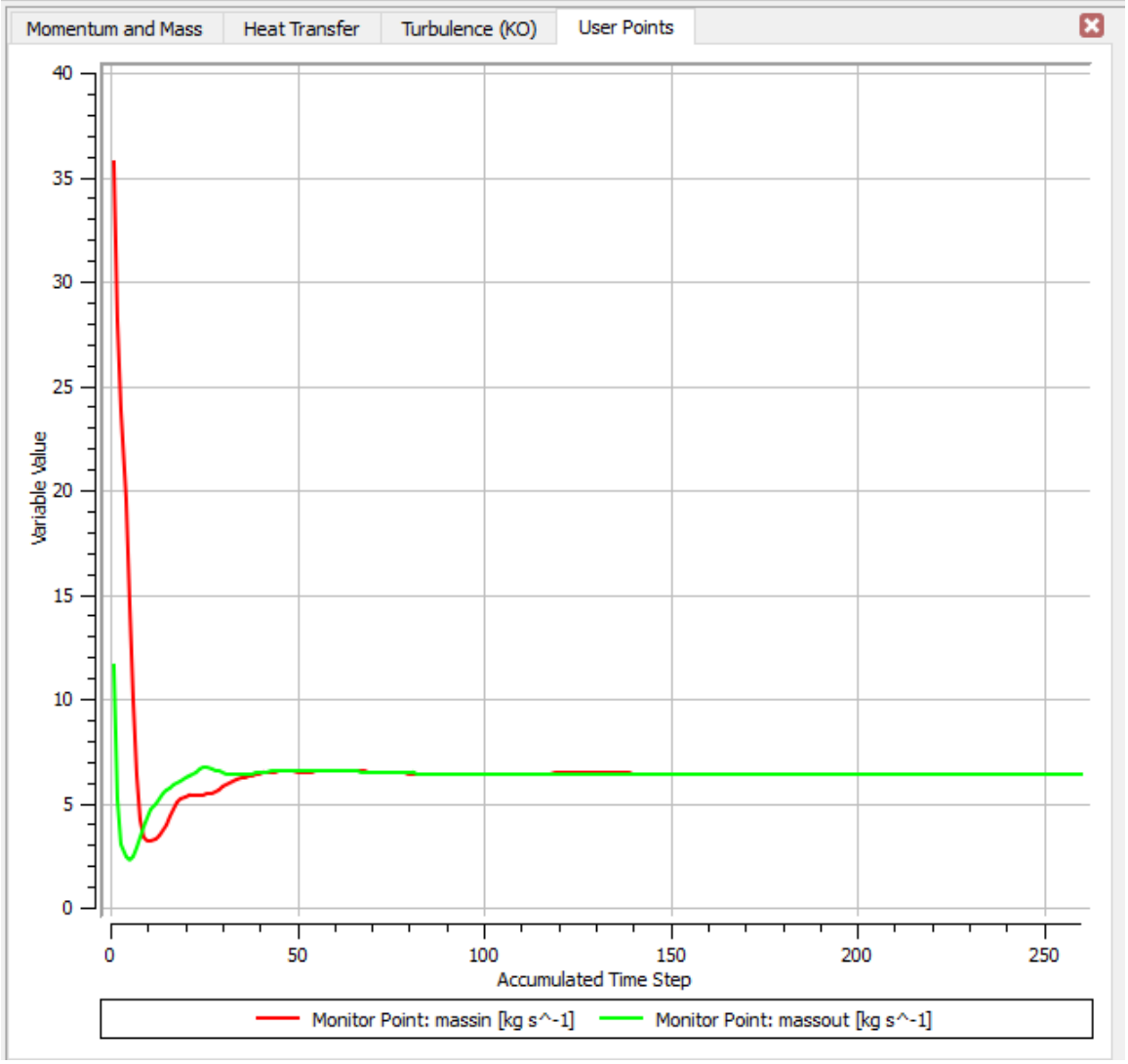

Figure 16. Mass flow as calculated from the user-defined expressions at the inlet and outlet

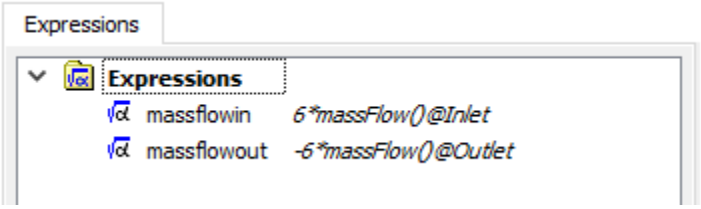

Figure 17. Mass flow expressions in CFX-Pre

The static and total pressures needed to be measured in the simulation at the same location as the experimental probes to calculate the mass flow rate in the same manner numerically and experimentally. To measure the static pressure, a point was inserted in the model on the wall of the bell mouth at the same location where the 6 static ports are located on the actual bell mouth. They are located 6 inches upstream from the surface where the bell mouth interfaces with the cone attachment. This is according to the ASME standard where the measurements should be taken one half of the throat diameter upstream from the exit plane [5]. To measure the total pressure, another point was inserted in the atmospheric air outside the bell mouth where the flow appears to be undisturbed by the flow into the bell mouth. This is close to the location where the total pressure is measured on the real TCR. The locations of these two points are shown in Figures 18 and 19. Additionally, Figure 18 shows the y+ values along the wall, showing a maximum y+ of 8.542. The y+ value is essentially a non-dimensionalized representation of shear stress at the wall and it indicates how well the simulation resolves the shear stress at the wall. This simulation used a standard k-ω turbulence model, which is valid for low Reynold's number calculations and the viscous sub-layer can be resolved to the wall.

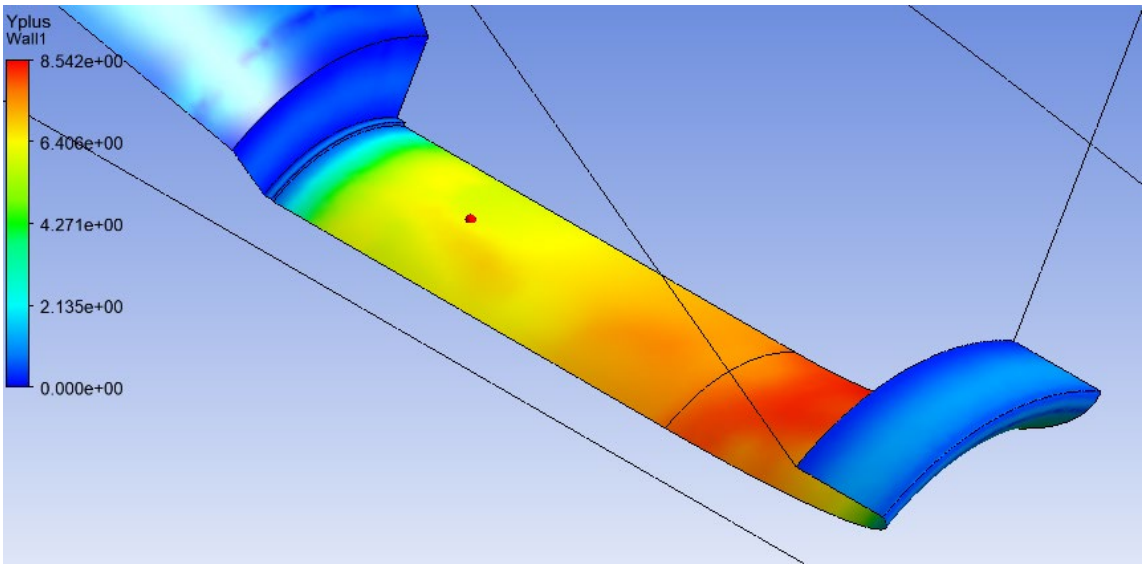

Figure 18. Static pressure port location along the wall of the bell mouth shown by a red dot.

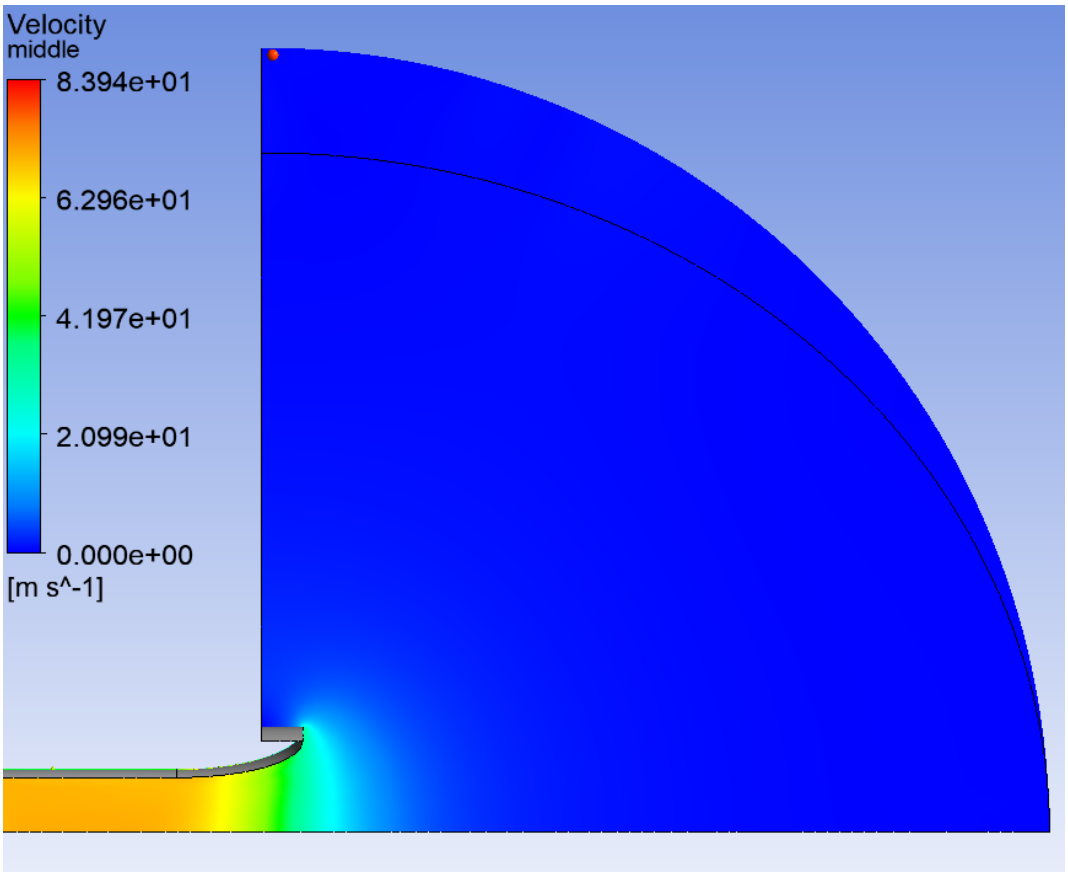

Figure 19. Total pressure port in atmospheric air undisturbed by flow into bell mouth

The plane bisecting the 60° wedge is shown with velocity as the color scale to show that the flow at the location where total pressure is measured is very nearly zero. The pressure measurement point itself is displaying pressure on a different color scale, therefore the color of the point has no correlation to the color scale shown.

C. SIMULATION RESULTS

The run as described produced realistic flow results through the model. Other parameters could be used to model different flow conditions including different pressure differentials simulating different compressor fan speeds and different throttle positions to restrict the flow. The parameters used in this run were a baseline for a rough comparison to the experimental data. The velocity of the flow through the geometry is shown in Figure 20 on a plane that bisects the 60° wedge.

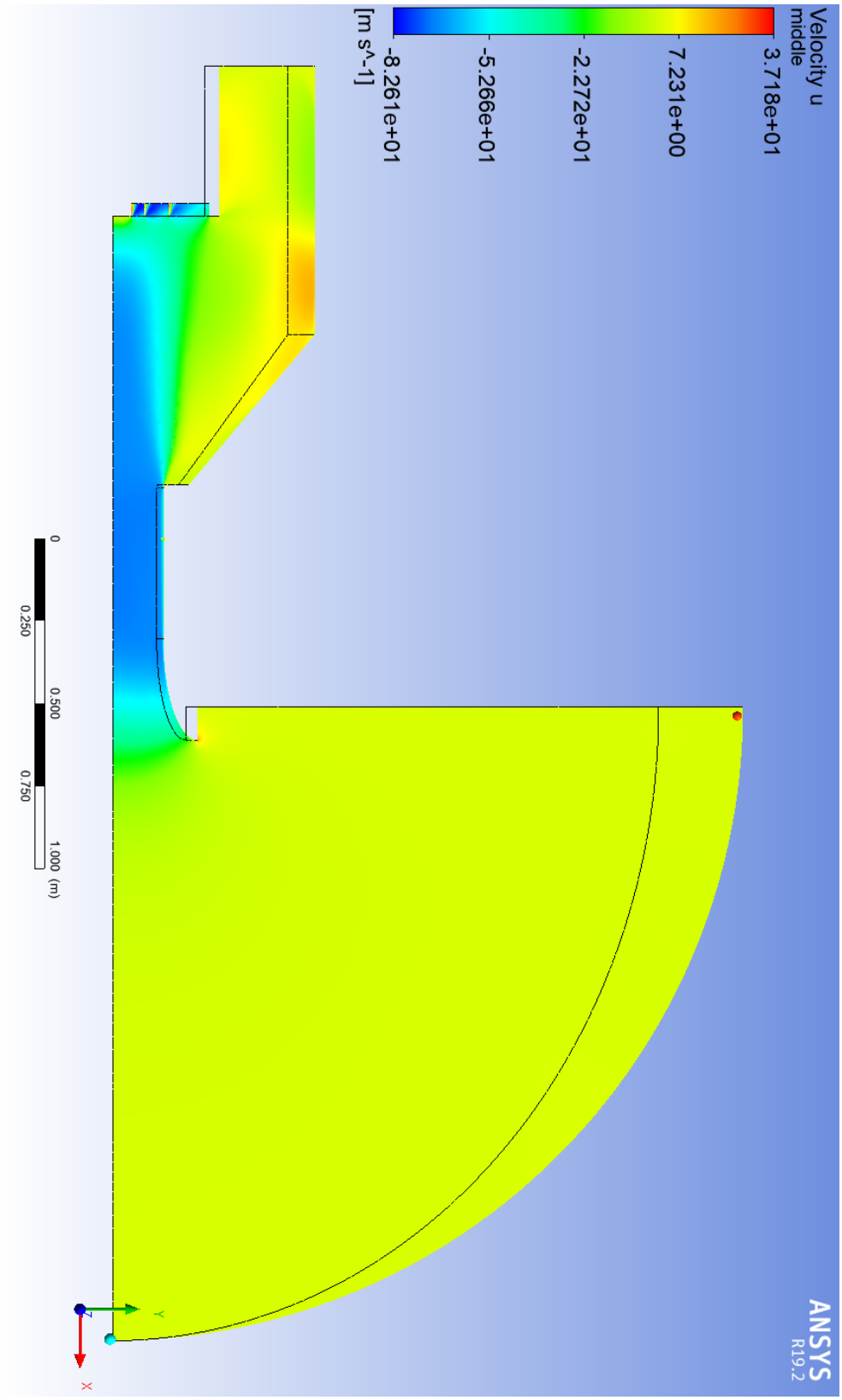

Figure 20. Velocity distribution through the entire geometry

Figure 20 shows the axial velocity through the model (velocity in the x direction). Flow moving from the inlet of the geometry to the outlet is defined as negative due to the choice of coordinate system shown by the axes in the lower right corner of Figure 20. The throttle is where the flow in the model is most restricted and most difficult to resolve computationally, so the profile of the flow through the throttle is important to consider. The entire cross section of the throttle shows the velocity exiting the outlet plane, and the side view of the plane bisecting the throttle shows the flow as it approaches the throttle. These two views are shown in Figure 21. As shown in Figure 21, there are regions in the throttle where flow is flowing back into the fluid domain. Positive velocities represent air flowing upstream. These pockets of back-flow fluctuate and produce disturbances in the convergence of the solution.

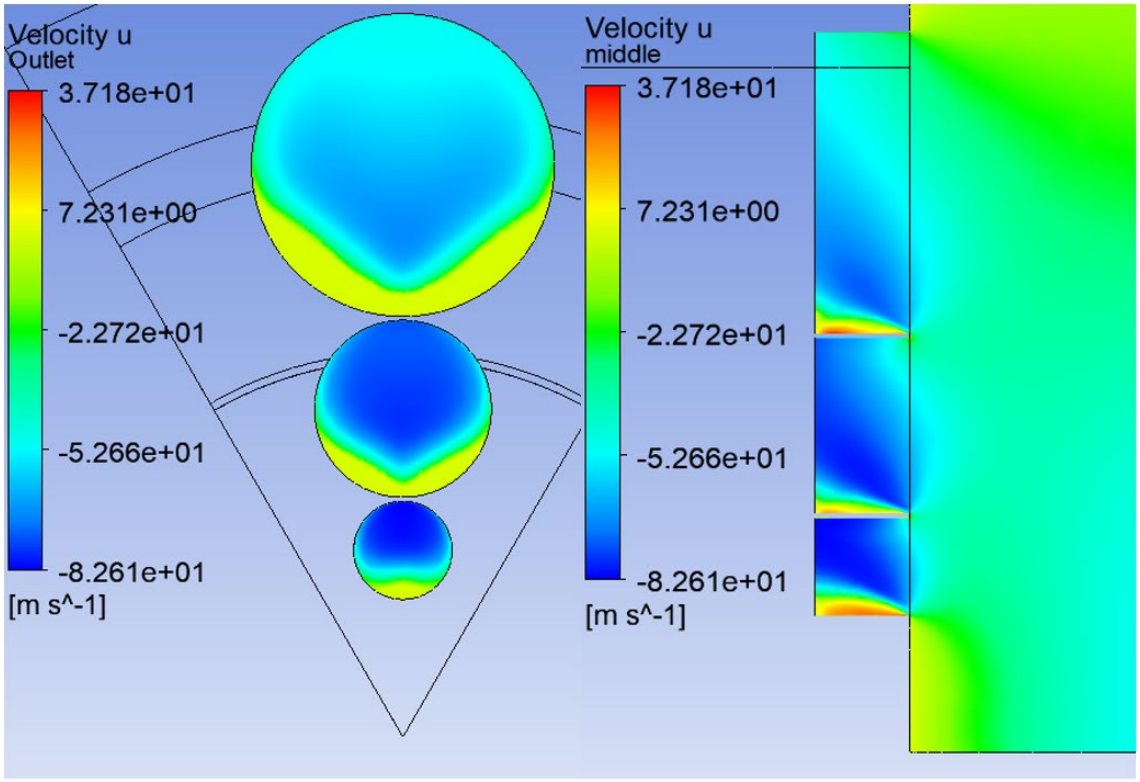

Figure 21. Flow through the throttle from side and front view

The data collected from the analysis that were to be used in the calculation of the discharge coefficient are tabulated in Table 2.

Table 2. CFD data used for discharge coefficient calculation

Flow Characteristic	Value
Throat Static Pressure	1.687 kPa
Total Pressure	5 kPa
Total Temperature	285 K
Density	1.3 kg/m3
Isobaric Specific Heat	1000 J/kg·K
Dynamic Viscosity	1.83×10^{-5} N·s/m^2
Mass Flow Rate	6.398 kg/s

The ideal mass flow rate was calculated using Equation 2 with the throat static pressure. The MATLAB script used for calculations can be found in the Appendix. The calculation assumed compressible flow and adjusted for that. The discharge coefficient which is the ratio of the calculated mass flow rate given by the CFX simulation to the calculated ideal mass flow rate was calculated to be 0.9647.

THIS PAGE INTENTIONALLY LEFT BLANK

IV. RAKE PROBE DESIGN

The CFD analysis provided an approximation of the flow in the bell mouth, but the objective is to measure the flow profile in the real bell mouth. The rake probe measures that real flow profile. The approximated flow profile from the CFD analysis gives insight into where the individual pitot tubes on the rake probe should be to most accurately measure the flow profile.

A. PROBE LOCATION CALCULATIONS

The real mass flow rate is measured with a rake probe that takes pressure measurements across the throat of the bell mouth inlet. Preliminary CFD simulations provided the velocity profile of the flow, which is ideally axisymmetric, shown in Figure 22. The velocity profile is normalized, with a velocity fraction of 1 being the maximum flow velocity and a radial position fraction of 1 being the inner radius of the bell mouth.

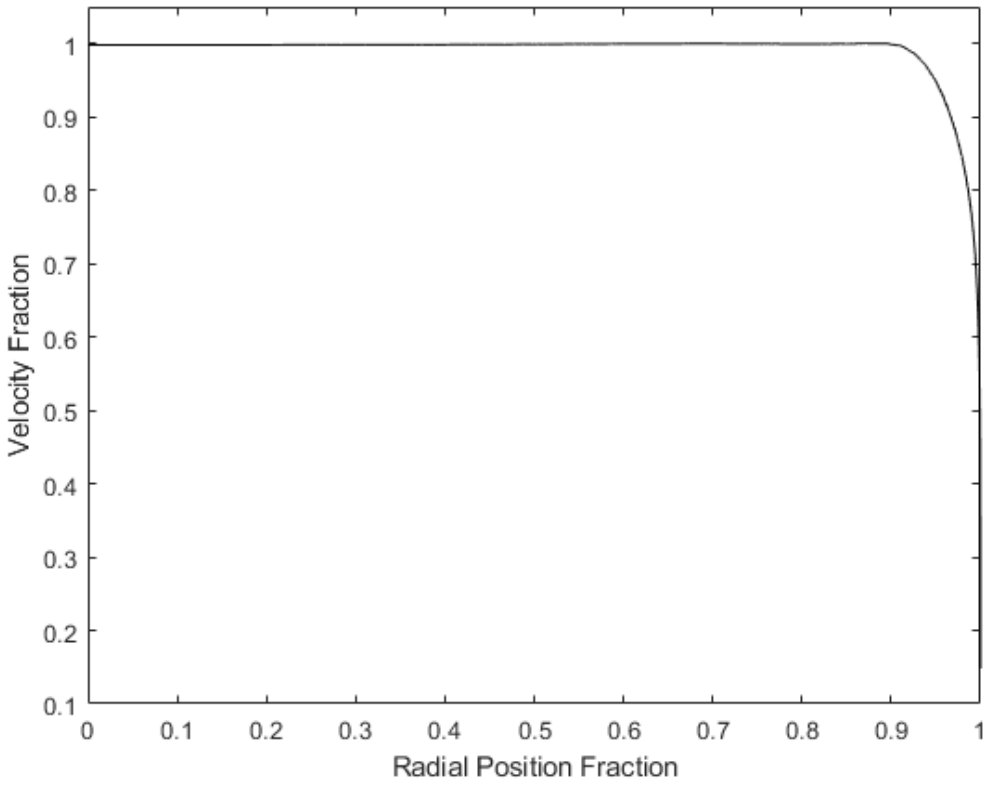

Figure 22. Velocity profile of flow through bell mouth inlet

The radial locations of the probes are chosen so that the curve connecting the data points most accurately follows the known velocity profile. A curve that follows the velocity profile as closely as possible results in an accurate mass flow measurement when that curve is integrated over the entire cross section of the inlet.

There are several restrictions on where the probes can be located that had to be taken into account. The tubing used for the probes has an outer diameter of 1.651 millimeters and the probes are mounted so that they are within the bell mouth inlet. Therefore, the closest a probe can get to the surface of the bell mouth is when the outside of the tube is resting against the bell mouth surface. In this condition, the center of that tube is 0.8255 millimeters from the wall. Due to the steep velocity gradient at the wall, even this small distance hinders the ability of the rake probe to accurately measure the velocity profile of the flow.

An additional hindrance is described in Pankhurst and Holder which specifies that two adjacent pitot tubes shall not be within two diameters of one another [6]. This is because as each probe stagnates the local flow in order to measure the total (or stagnation) pressure, it creates a disturbance in the flow. That disturbance will impact the measurements at the adjacent probes if they are closer than the Pankhurst and Holder guidance allows [6]. To get around this, the probes are alternated between both sides of the rake probe to take advantage of the symmetry of the flow. Additionally, this allows for validation of the symmetry of the flow, as both sides should independently produce the same result.

The initial spacing of the pitot tubes was based on a cosine distribution. First, 15 angles evenly spaced between 0° and 90° were computed. The cosine of each of these 6° slices became the normalized radial location for the pitot tubes. Each 6° slice and its cosine component projected onto the abscissa is shown on Figure 23. As shown in Figure 23, using this distribution, the probes would be closer together near the ends of the rake and farther apart near the center. This makes the cosine distribution a good first design, as the closer together probes will be near the wall where there is a steep velocity gradient.

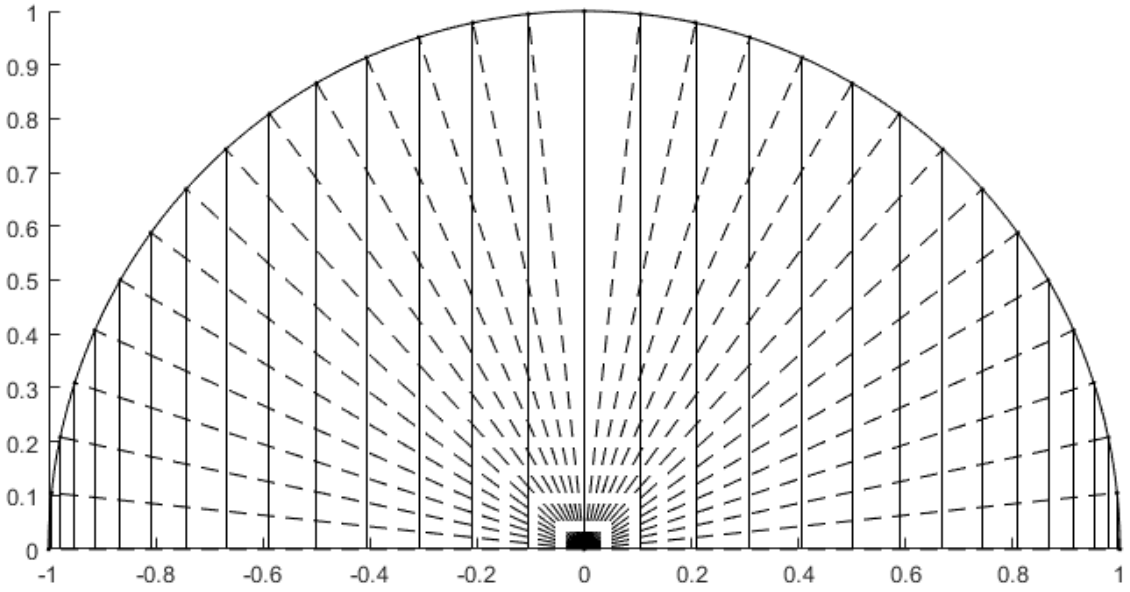

Figure 23. Cosine distribution for use in rake probe spacing

The inner radius of the bell mouth inlet is 0.1524 meters, but to properly locate the center of each probe, the diameter of the probes themselves must be taken into account. The adjusted inner radius becomes 0.1516 meters. The normalized radial location of 1 (cosine of 0°) becomes 0.1516 meters from the center of the flow. The locations of the probes based on this cosine distribution projected onto the previous velocity profile are shown in Figure 25. This serves as a baseline for calculating the uncertainty of the mass flow measurements from the rake probe.

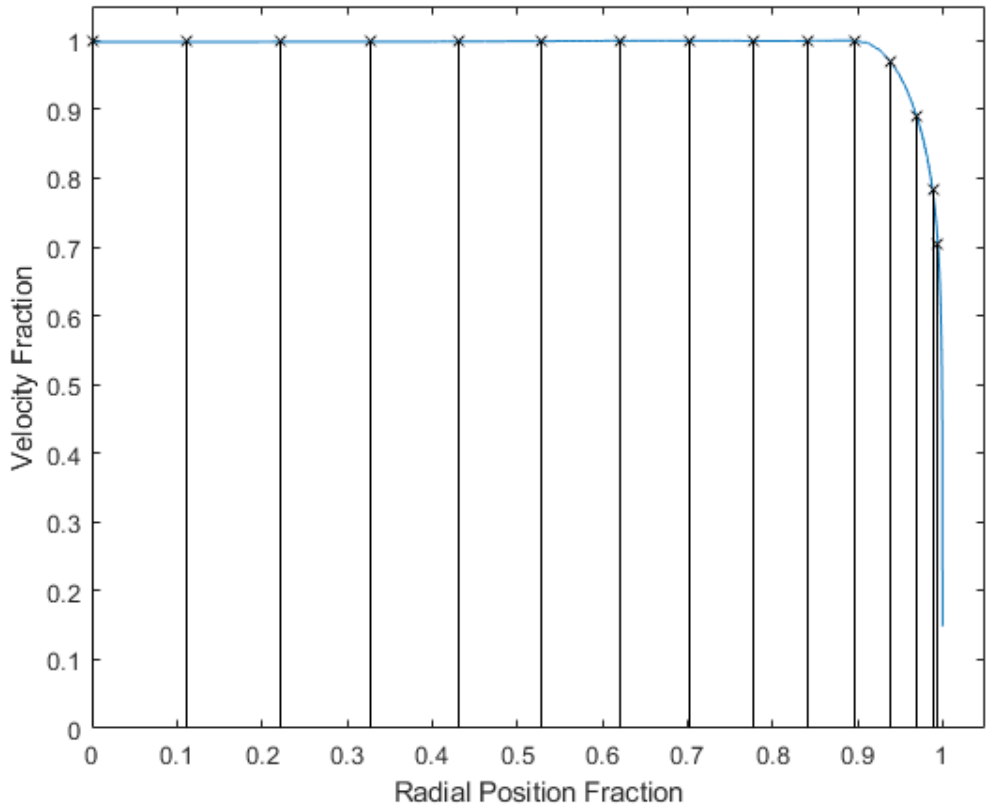

Figure 24. Cosine probe distribution projected on the velocity profile

The hypothetical mass flow from this velocity profile is calculated by integrating the velocity of the flow over the area of the bell mouth inlet, as shown in Equation 4

$$\dot{m} = \int_0^R 2\rho\pi v dr\,, \tag{4}$$

where r is the radial position in meters and R is the radius of the bell mouth in meters. The CFD provided the standard to which the mass flow calculated with the probes was compared to calculate the uncertainty of the mass flow value. The pitot tubes provide pressures at discrete points in the flow and corresponding velocity values are derived from those pressures. The segments of the profile in between the discrete points must be approximated to calculate the mass flow. This approximation was done in multiple ways to check their validity. The first way was to approximate the profile with straight lines between the discrete points, which results in a trapezoidal integration scheme. Due to the

velocity profile being concave down, the trapezoidal integration will always underestimate the mass flow rate, but the error is consistent and can be calculated. The discrete radial locations of the probes and their corresponding velocities were also used to create a spline, which could then be integrated with respect to radius from 0 to R. These calculations with actual data are covered in the calculations section in more detail, but they are mentioned here because they aided in the selection of the locations for the probes.

After using the cosine spacing as a first design iteration the spacing was then adjusted to better match the CFD velocity profile. From the center of the flow to approximately 90% of the radius, the flow is approximately uniform, while from 90% to 100% of the radius is changes dramatically. This is expected, as the boundary layer caused steep velocity gradients near the wall. Having probes close together in the section of the flow with the most change would help more accurately measure the flow. The spacing is limited, as previously mentioned, by the Pankhurst and Holder criterion of two diameters between probes. With half the probes on one side of the flow and the other half on the opposite side, every second probe must comply with the two-diameter spacing. One half of the probes will be referred to as the "port" side probes and the other half will be referred to as the "starboard" side probes. These names will help distinguish between the sides but makes no reference to their actual locations in the flow because the orientation of the probe will change. Therefore, if the two sides were overlapped, the spacing between probes in this section would be much closer than two diameters, allowing the measurements to be more accurate.

The location of each probe was calculated based on these criteria so that this close spacing extended from 100% of the radius to approximately 83% of the radius, to be sure that the rapidly changing section of the velocity profile was covered. One probe on each side was placed at 75% of the radius as a comparison point between the two sides to visualize if the flow is indeed axisymmetric. Two other probes were equally spaced between the center of the flow and the beginning of the close spacing to cover the approximately uniform section of the velocity profile. The final probe was placed such that it passed directly through the center axis of the bell mouth.

Table 3. Location of each probe relative to flow center in meters

1	2	3	4	5	6	7	8
0	0.0423	0.0845	0.1143	0.1143	0.1268	0.1299	0.1318

9	10	11	12	13	14	15	16
0.1349	0.1367	0.1398	0.1417	0.1448	0.1466	0.1497	0.1516

The individual port and starboard locations are shown in Tables 4 and 5. The layout of these probe locations on the previous velocity profile from the CFD analysis is shown in Figure 25 to display their proximity to one another.

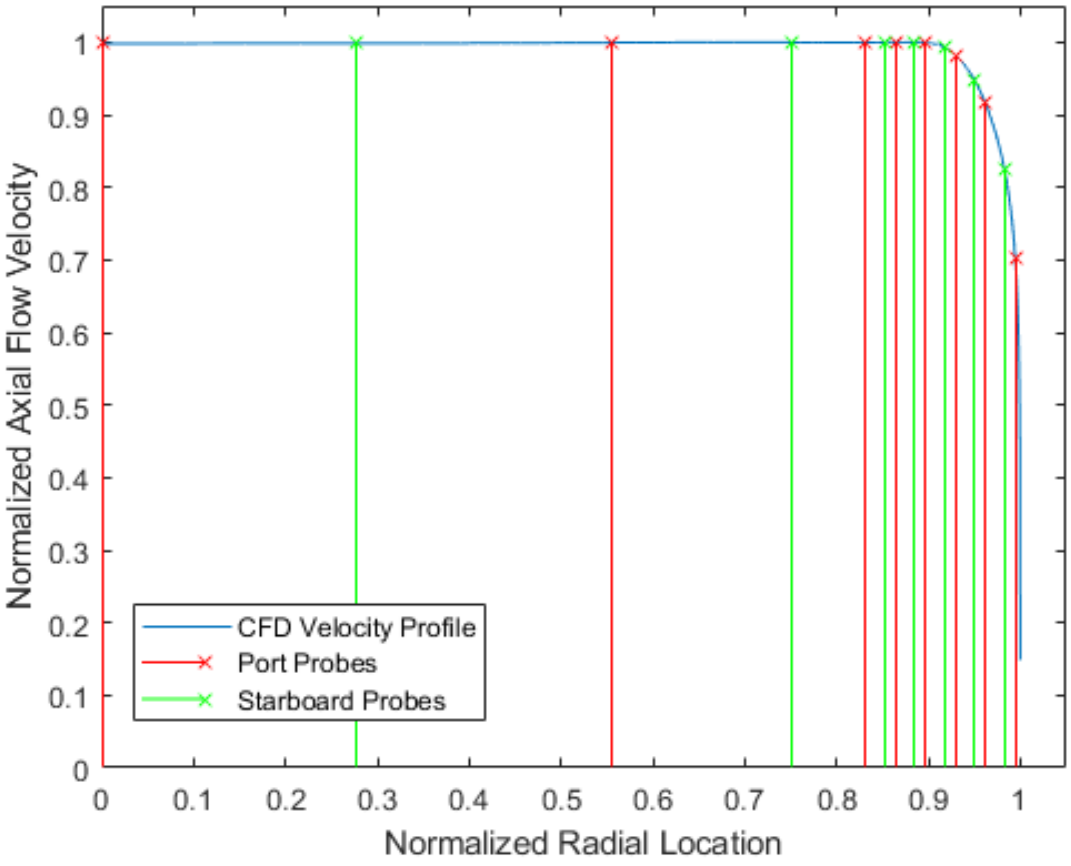

Figure 25. Port and starboard probes and their positions relative to flow center

Table 4. Port probe locations relative to flow center in meters

1	2	3	4	5	6	7	8	9
0	0.0845	0.1143	0.1268	0.1318	0.1367	0.1417	0.1466	0.1516

Table 5. Starboard probe locations relative to flow center in meters

1	2	3	4	5	6	7	8
0	0.0423	0.1143	0.1299	0.1349	0.1398	0.1448	0.1497

B. DESIGN OF FINAL RAKE PROBE

The rake probe had certain requirements needed to accomplish the desired task. First, it was to hold the individual pitot tubes rigidly in their respective positions. Secondly, it was to minimally impede the flow. Third, it needed to be rigidly mounted and have sufficient stiffness to retain its structural integrity even when exposed to high-speed air flow. The final rake probe was manufactured using a combination of traditional and additive manufacturing. The main structural piece of the rake probe is an aluminum bar 9.525 millimeters thick, 19.1 millimeters wide, and 330.2 millimeters long. A mill was used to drill holes in the bar that would house the pitot tubes. The bar had sufficient length to span the entire diameter of the bell mouth inlet and have enough on the ends to be mounted to brackets out of the flow. This bar was calculated to have a maximum deflection of 1.5e-8 meters while subject to a flow of 100 m/s, which is sufficiently small for the purposes of this study. The configuration of the mounted rake probe as viewed from the downstream side is shown in Figure 26.

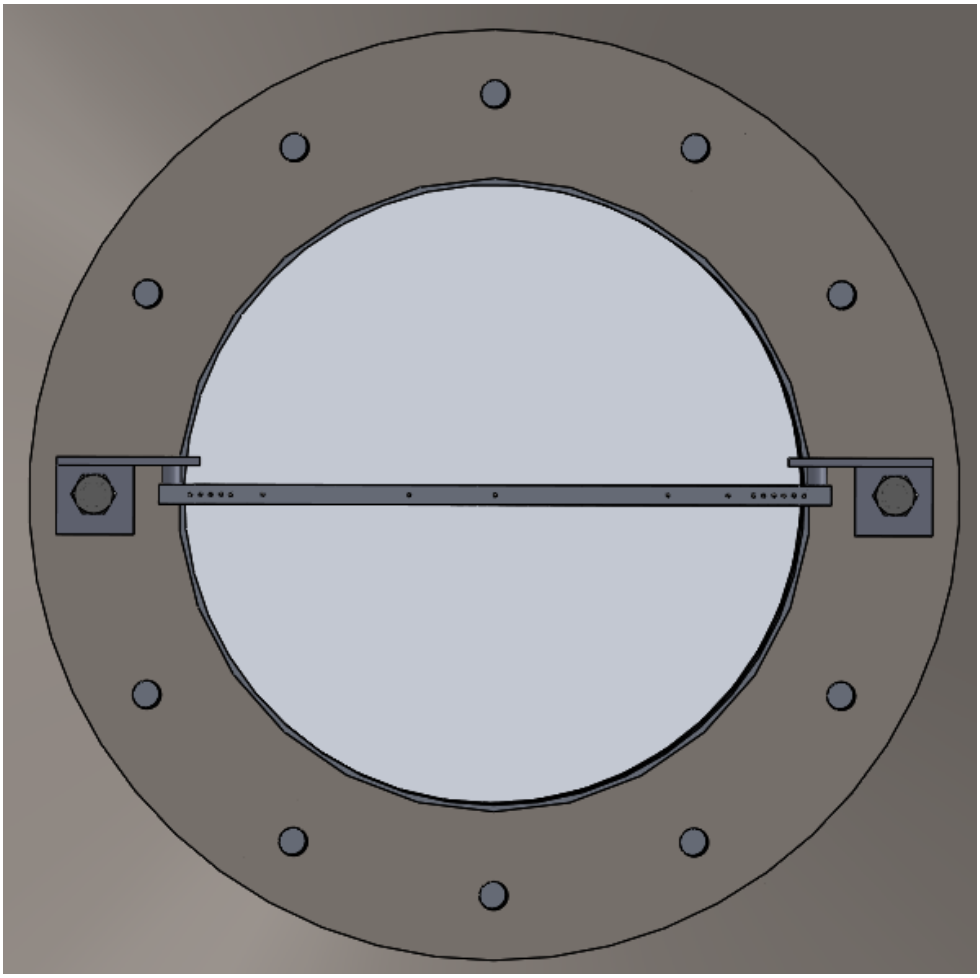

Figure 26. Mounted rake probe as viewed from downstream

The pitot tubes were to extend 0.0635 meters from the leading edge of the bar into the bell mouth. This would make the tubes highly susceptible to bending or otherwise displacing them from their desired locations. The mass flow rate calculations relied on accurate measurement of the locations of each probe, so they needed more stability than just the aluminum bar could provide. The other main hindrance was the effect of the blunt leading edge on the flow. Though the bar is slender, the leading edge was perpendicular to the flow creating non-optimal drag conditions. The solution to both of these problems came from an additively manufactured leading edge that would mount to the leading edge of the Aluminum bar, shown in Figure 27.

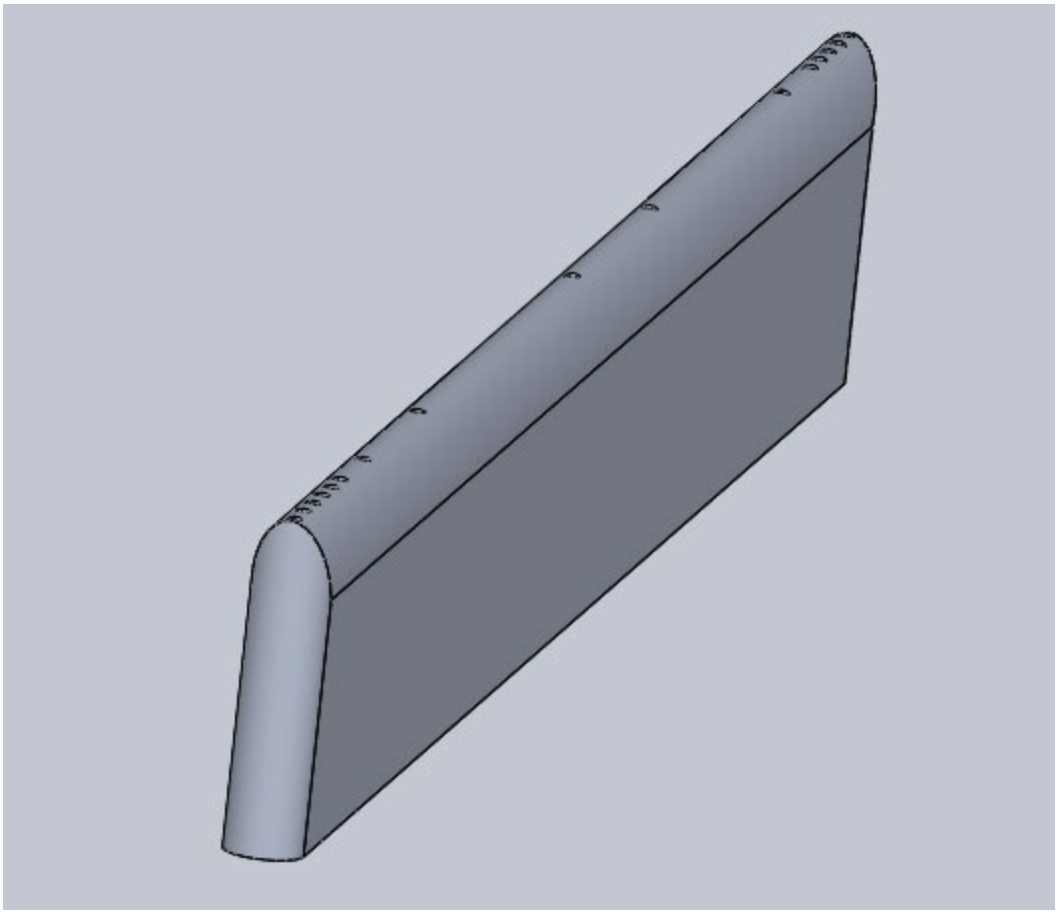

Figure 27. Additively manufactured leading edge to attach to rake probe

This new piece featured a 2:1 elliptical leading edge which provided more favorable flow conditions than the blunt leading edge of the bar itself. The piece also was printed with channels in each pitot tube's exact location along the length of the rake probe. The new leading edge extends 0.0413 meters forward of the Aluminum bar, so the channels provide much more stability to the individual probes than the bar alone. This leading edge was additively manufactured in two pieces in order to fit on the build plate. The part is made of PLA filament. The Solidworks model of the assembled rake probe is shown in Figure 28 and the Solidworks engineering drawing with the distance of each probe from flow center is shown in Figure 29. The distances shown in Figure 29 are equivalent to center-to-center distances.

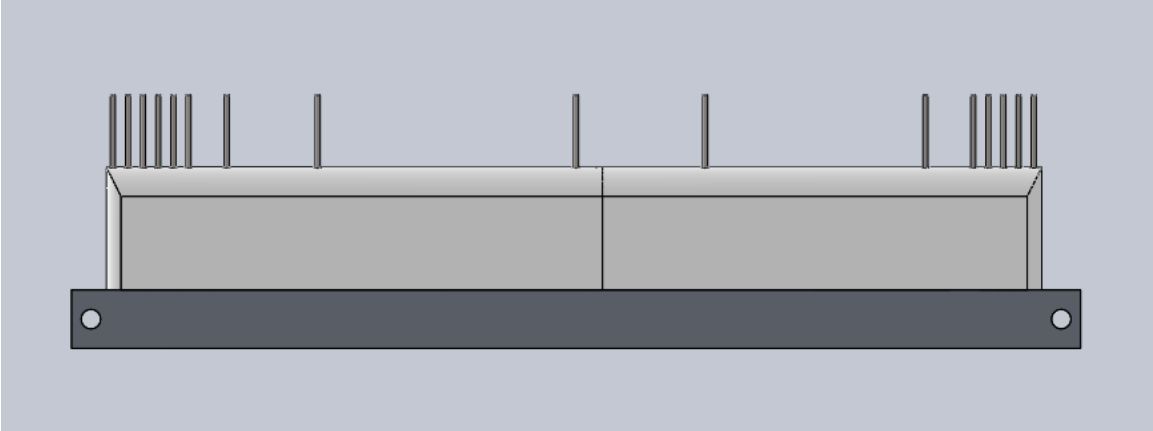

Figure 28. Model of the fully constructed rake probe

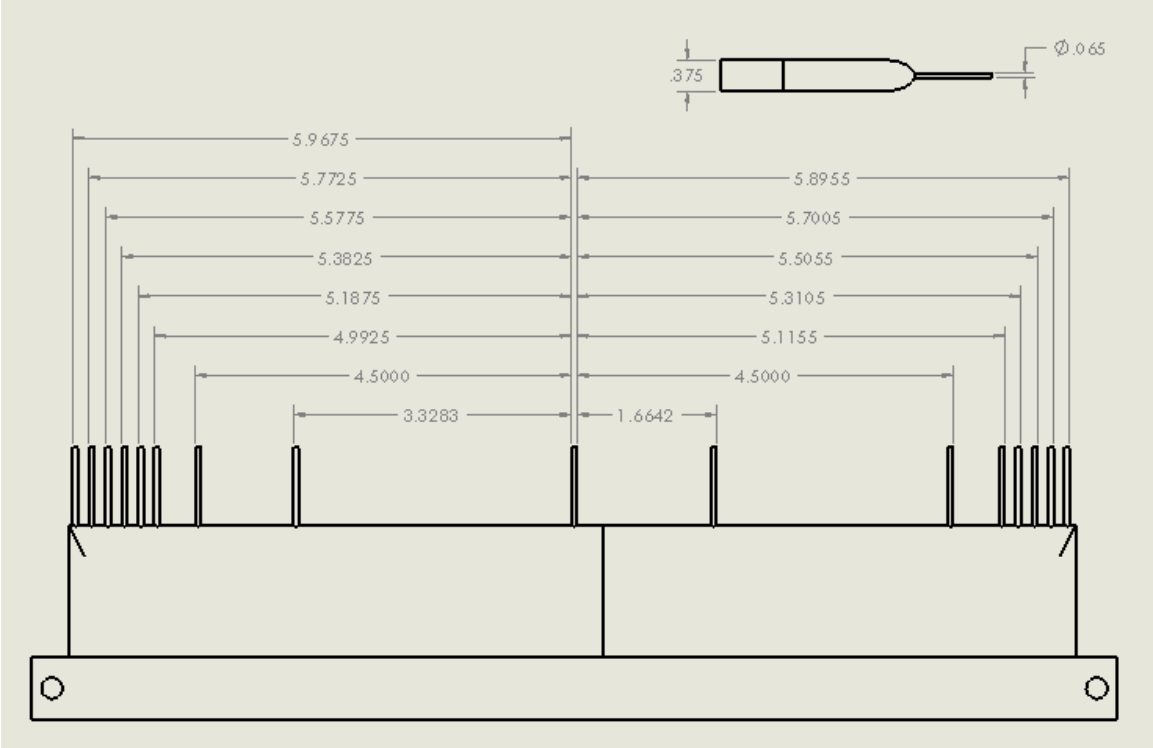

Figure 29. Engineering drawing of assembled rake probe with probe spacings

The fully constructed rake probe is shown in Figure 30. The back end of the pitot tubes come out of the aluminum bar where they can be redirected to be best kept out of the flow.

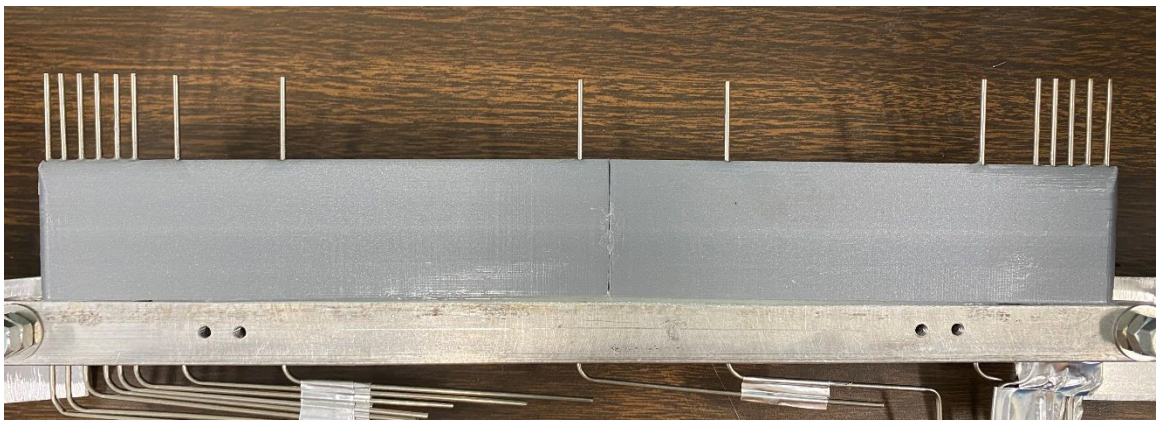

Figure 30. Top view of the assembled rake probe

The side view of the leading edge of the rake probe with the probes protruding from the front is shown in Figure 31. This view shows the 2:1 elliptical leading edge and how much of the probe is supported by the additively manufactured piece.

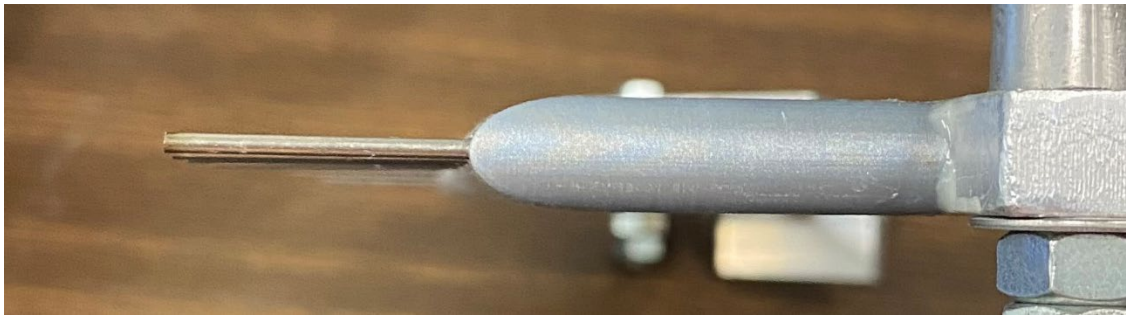

Figure 31. Side view of rake probe leading edge

After the rake probe was fully assembled, the location of each probe was measured using calipers with a precision of ±1.27e-5 meters. The probe furthest from flow center was to be in contact with the inner wall of the bell mouth. The locations of each probe are the center of that probe, so the probe in contact with the inner wall should have been 0.1515 meters from flow center. Each probe location was made relative to that furthest probe so that their actual location in the flow was accurately reflected. These actual locations relative to flow center for port and starboard sides are shown in Tables 6 and 7, respectively.

Table 6. Port probe locations relative to flow center in meters

1	2	3	4	5	6	7	8	9
4.7e-4	0.0848	0.1149	0.1273	0.1326	0.1376	0.1422	0.1470	0.1515

Table 7. Starboard probe locations relative to flow center in meters

1	2	3	4	5	6	7	8
-4.7e-4	0.0421	0.1143	0.1295	0.1346	0.1396	0.1445	0.1496

These actual locations are shown on Figure 32 for comparison to Figure 25.

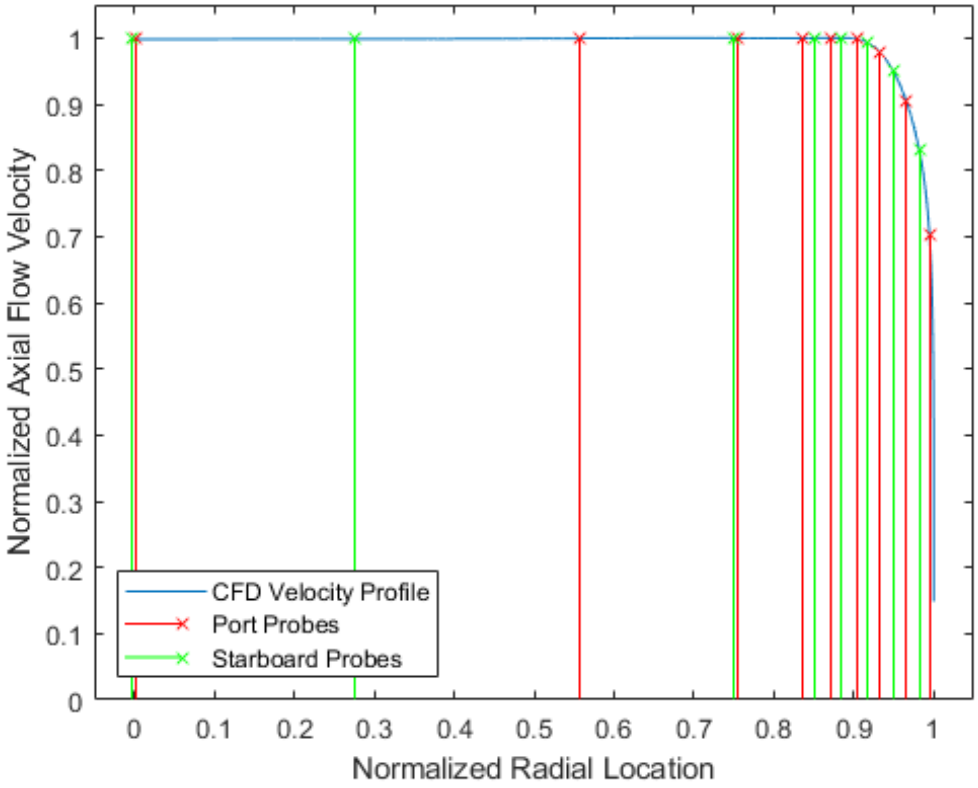

Figure 32. Location of port and starboard probes on the assembled rake probe

V. BELLMOUTH AND THROTTLE CASING IMPLEMENTATION

The design of the bell mouth as well as the throttle casing was done by Wallen [4]. In order to implement these components onto the TCR, a structure was required to support the parts. The throttle casing fully encompasses the throttle, which occasionally needs to be accessed for instrumentation and maintenance. The throttle casing is bolted to a plate behind the throttle with 24 bolts, creating an airtight seal so that all air coming into the system is through the bell mouth. When the throttle needs to be accessed, however, the throttle casing would be detached from that plate and pulled away. Therefore, the throttle casing and bell mouth needed to be supported in such a way that allowed them to be unbolted and pulled away from the throttle and then mounted again easily. The conclusion was for the whole assembly to rest on leveling jacks with wheels and swivel casters.

A. SUPPORTS

The throttle casing and bell mouth are made from stainless steel and aluminum, respectively. The entire assembly is 2.032 meters long and 0.8128 meters wide. The support structure had to be mounted to the assembly in such a way that would keep it stable while moving on and off the throttle. The basis of the structure was to have a 0.0762-meter x 0.0762-meter hollow aluminum support beam mounted along the length of the assembly with four metal supports attaching to the throttle casing at the two flanges on either end of the casing.

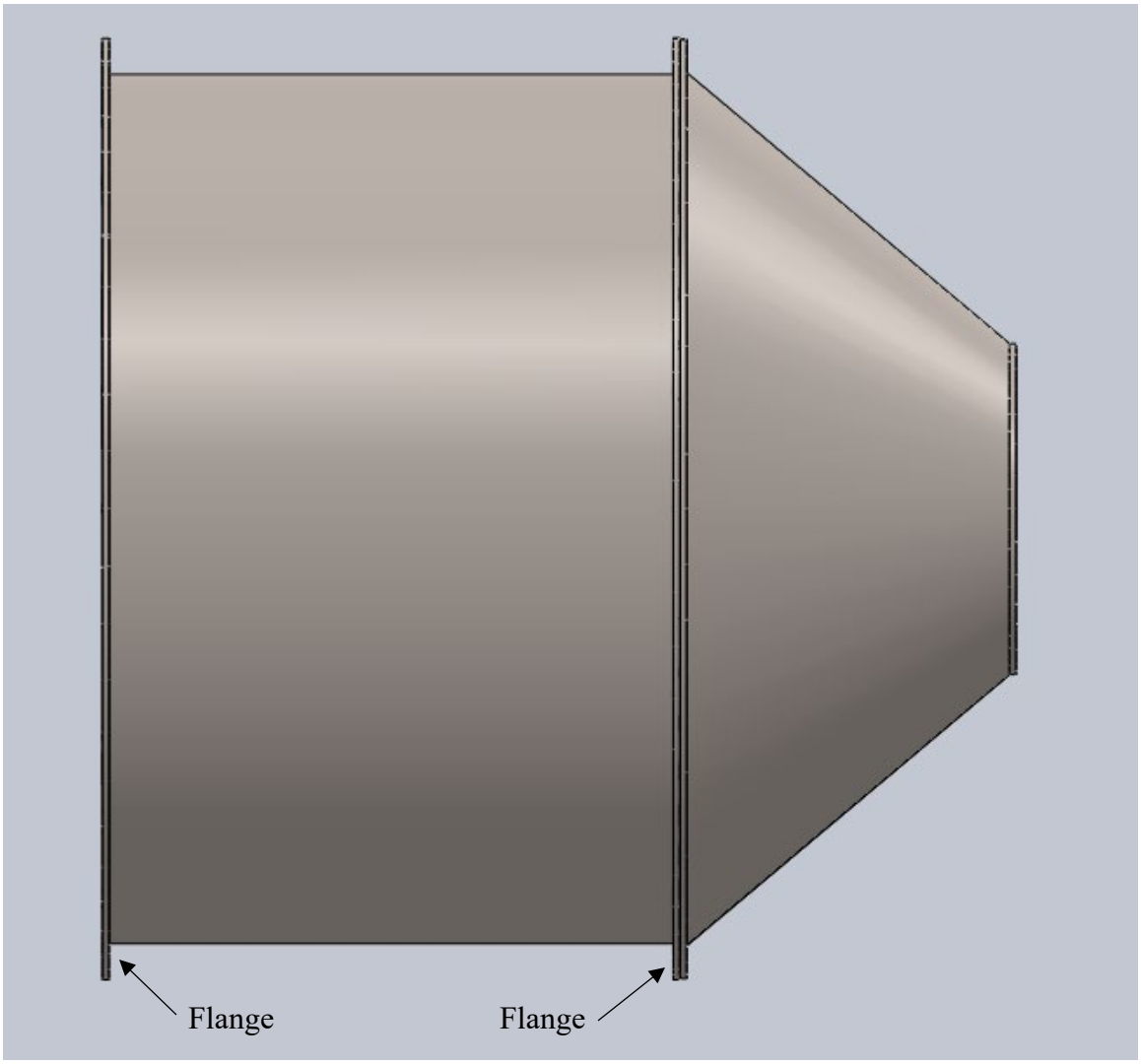

Figure 33. Throttle casing including the cone attachment

The throttle casing consists of the casing itself and the cone attachment that connects the large diameter casing to the smaller diameter bell mouth. The two ends of the casing consist of flanges, shown in Figure 33, approximately 0.0508 meters wide with 24 evenly spaced bolts around the entire circular casing. These were the easiest locations to mount supports to the casing; however, the cone attachment and bell mouth would both be attached outside the two supports. This is cause for concern because if the center of mass was outside the supports, the assembly would be prone to tipping. This could be remedied by locating the leveling jacks that will rest on the ground in such a way that the center of mass is between them, but it would still cause unnecessary stress on the supports and the

bell mouth, which would be cantilevered. Accurate location of the center of mass would determine if another support would need to be placed under the bell mouth. The location of the center of mass of the throttle casing, cone attachment, and bell mouth is shown in Figure 34.

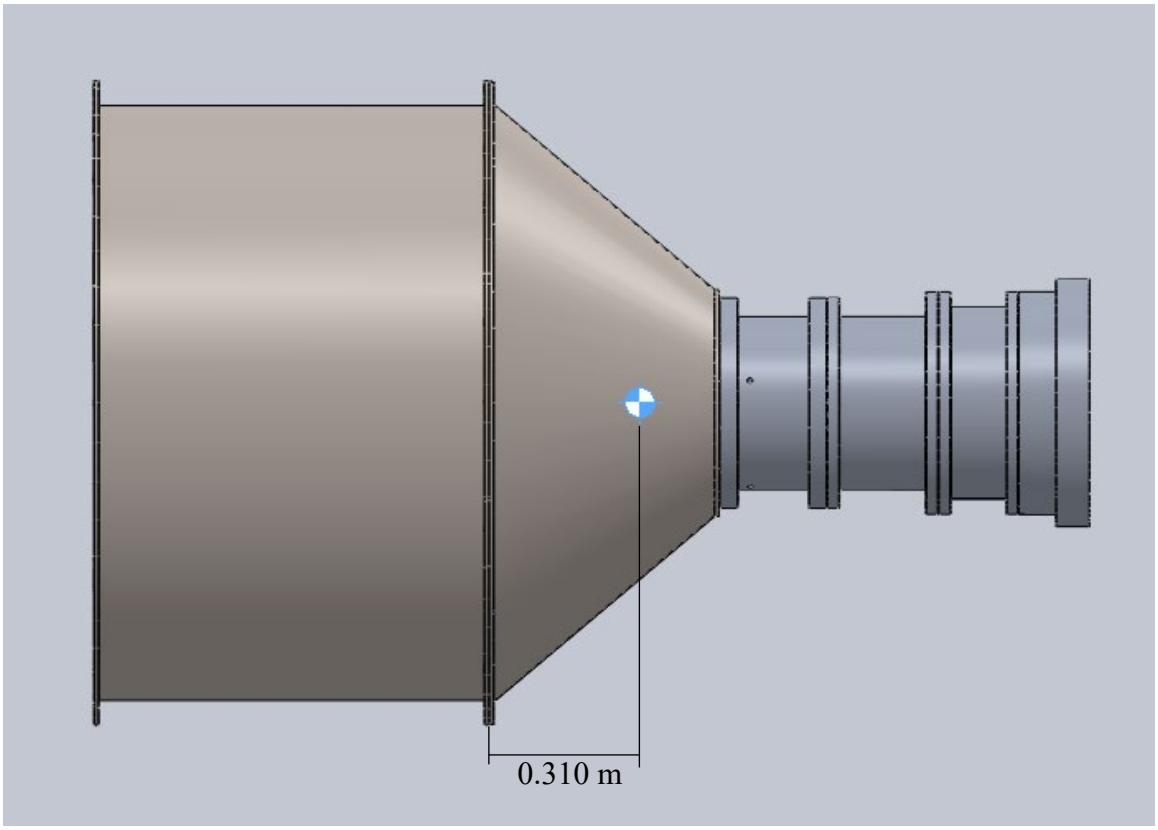

Figure 34. Center of mass of the assembly

The center of mass was calculated to be 0.310 meters to the right of the nearest throttle casing flange. For this reason, another support would need to be placed under the bell mouth so that the entire assembly is supported.

The supports attaching to the throttle casing flanges were to mount to multiple bolts and then mount to the support beam so that the beam would be a proper height for the leveling jacks to be mounted. The designed support on the throttle casing flange as seen from the upstream side is shown in Figure 35.

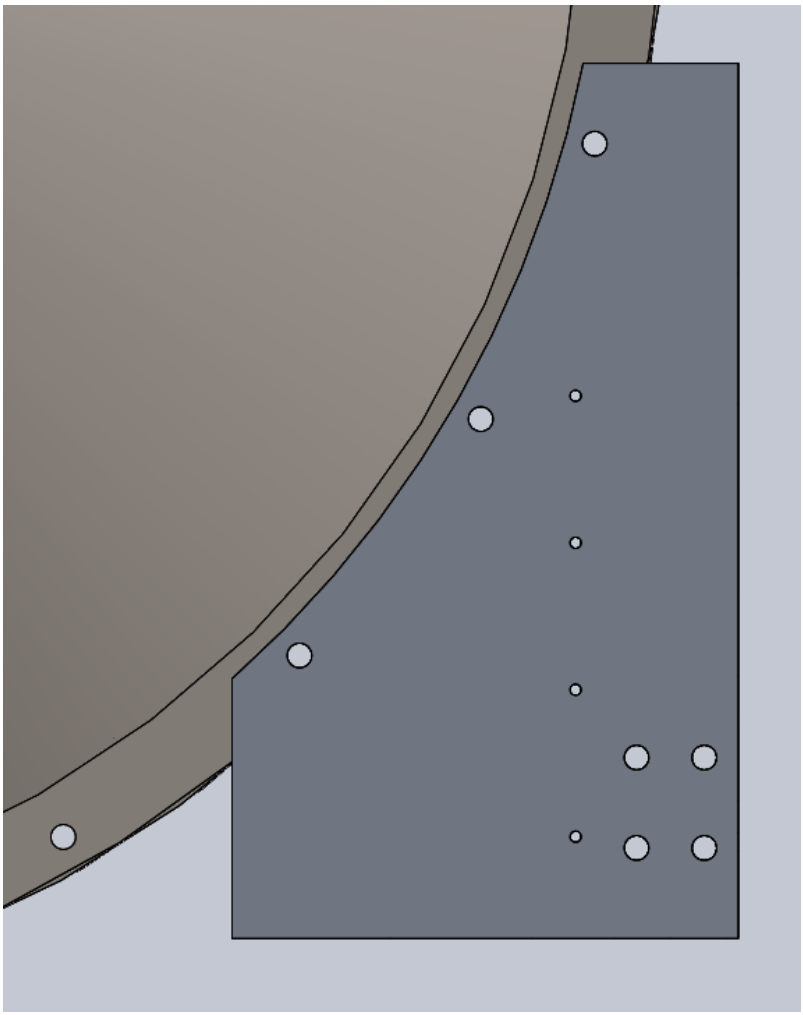

Figure 35. Support attached to throttle casing flange

Attaching the support to three bolts on the flange allows for distribution of the load while also keeping the size of the support reasonably small. The material used for the supports was 9.525-millimeter-thick aluminum. In order to make the support less susceptible to buckling, they were mounted to the beams using a piece of angle iron on both sides that extends 0.1524 meters up the support, 0.1524 meters along the beam, and is 0.0762 meters wide (same as the width of the beam). Four bolts hold both angle irons and the support together, then four more bolts hold each individual angle iron to the beam. One of the supports mounted with the angle irons to the beam is shown in Figure 36.

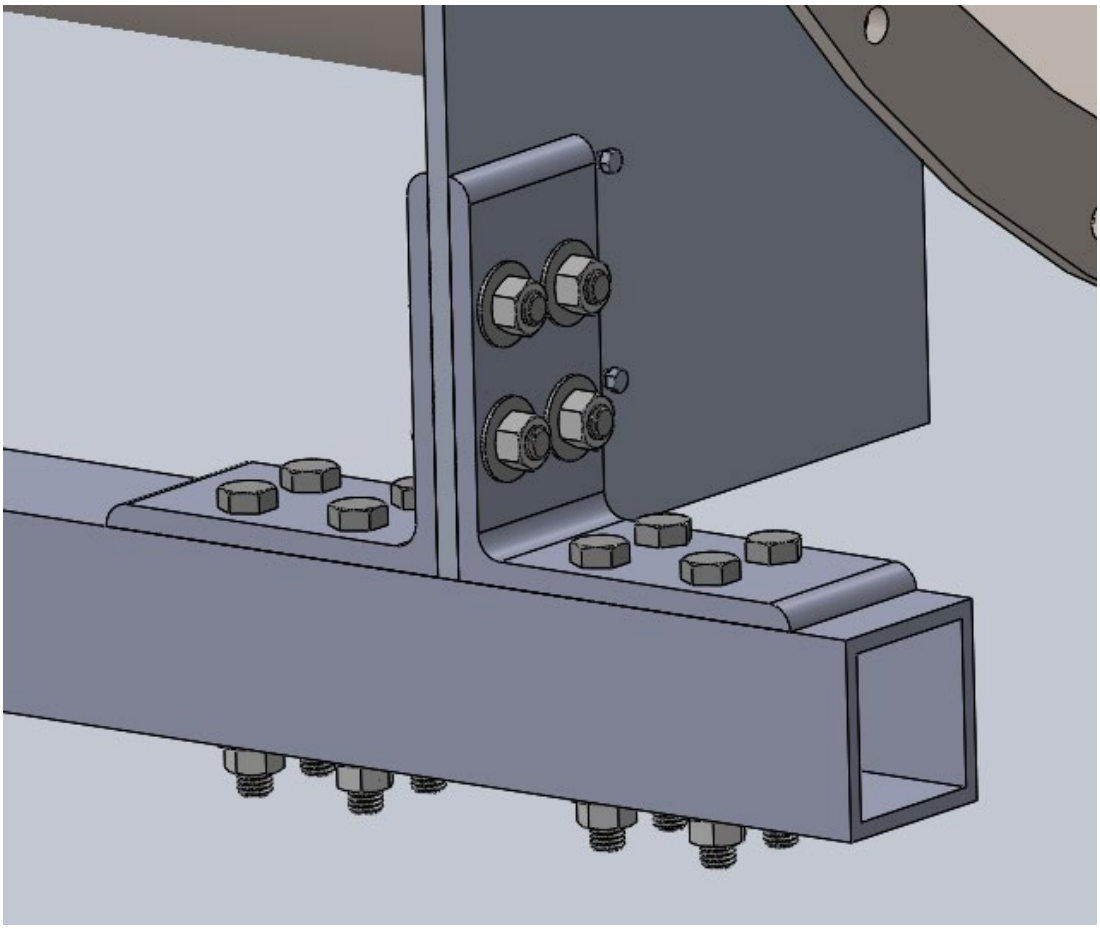

Figure 36. Support mounted with angle irons to the support beam.

This configuration was duplicated for each of the four flange-mounted supports. This throttle casing, bell mouth, and support structure is expected to remain part of the TCR for many years, so longevity was the primary concern. The load on the supports was not enough to cause concern for buckling. However, over more years and more design iterations, should more equipment be added or the supports be repeatedly loaded and unloaded, stiffening components would provide extra protection against buckling. Segments of aluminum angle iron measuring 0.0254 meters x 0.0254 meters and spanning the height of the supports were added to either side of each support. The two angle iron segments and the support were all attached with four bolts. The support with the side-mounted angle iron braces is shown in Figure 37 and the full assembly of the throttle casing, bell mouth, supports, and beams is shown in Figure 38.

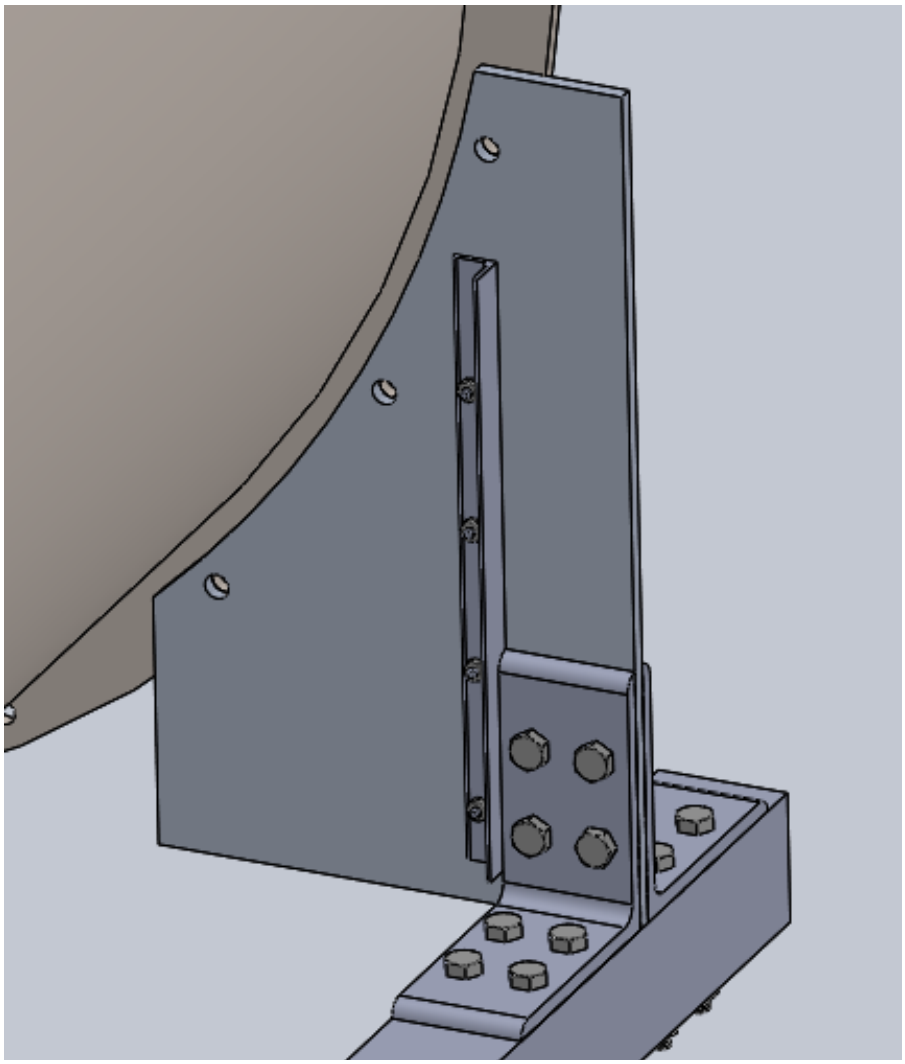

Figure 37. Support with buckle-preventing angle iron segments.

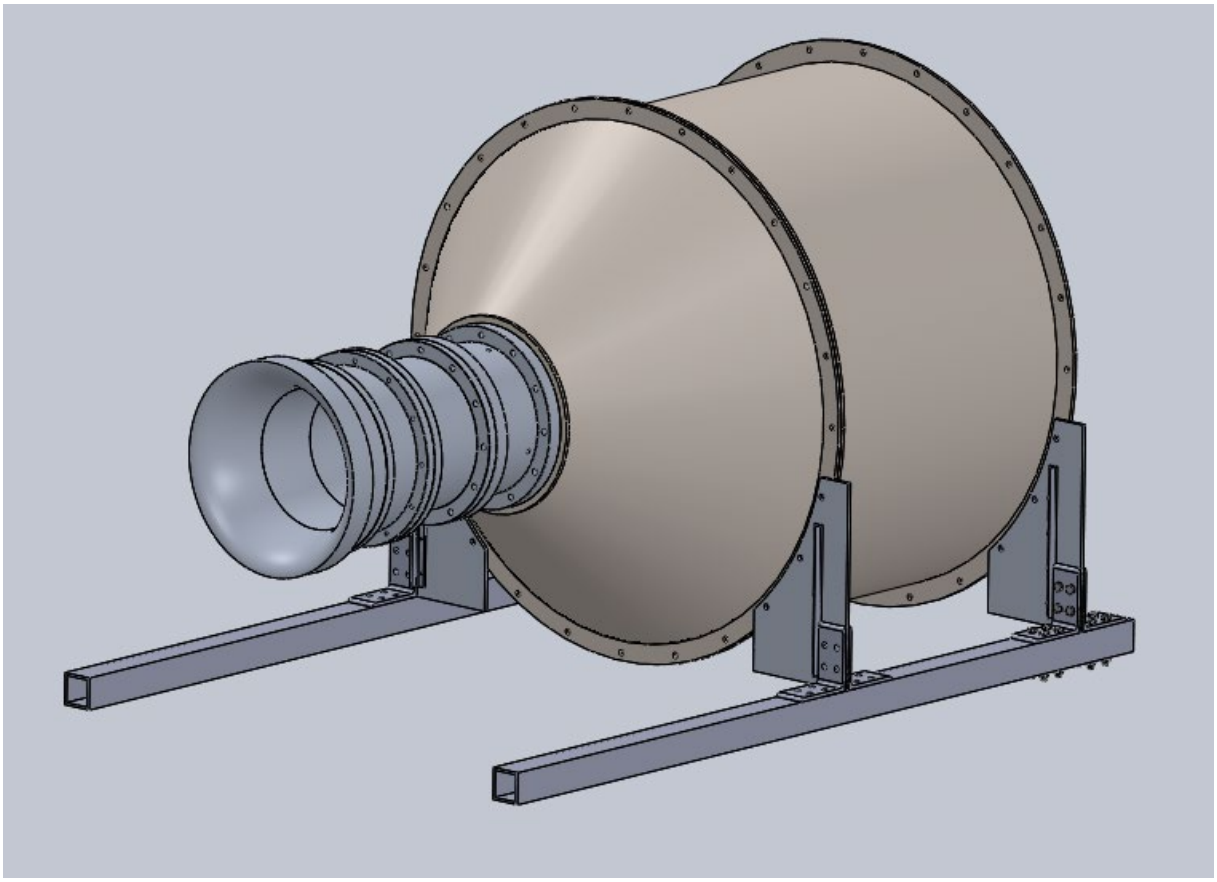

Figure 38. Assembled support structure.

B. BELL MOUTH SUPPORT

With the support structure assembled, the problem of the center of mass being forward of the forward most supports still exists. The bell mouth would need to be supported. To accommodate this, another beam was introduced, spanning from one beam to the other, under the bell mouth. A shorter segment of beam was then placed vertically on that new beam, supported on either side by angle irons. This configuration is shown in Figure 39.

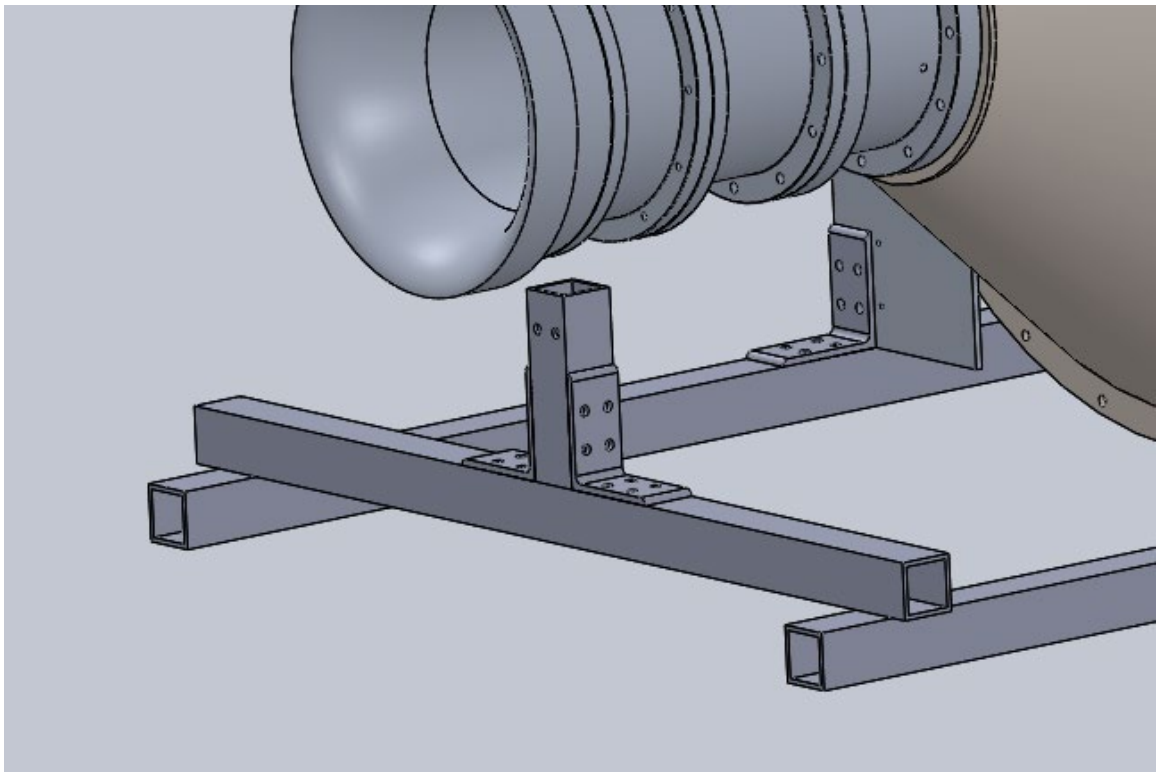

Figure 39. Support structure under bell mouth.

This structure provided a base for the bell mouth to be supported. The last piece that attached this structure to the bell mouth was cut to the right length once the entire bell mouth assembly was in place. The manufactured structure installed with the actual bell mouth is shown in Figure 40.

Figure 40. Bell mouth support after installation

C. WHEELED LEVELING JACKS

The throttle casing and bell mouth being properly supported was necessary, but more was needed from the support structure. The throttle would need to be accessed, which would require the throttle casing and bell mouth to be removed entirely, and then placed back around the throttle. It was decided that the support structure would be mounted on wheels that would allow the entire assembly to be rolled away from the throttle and rolled back onto it. The tarmac where this assembly would be placed is not level, so adjustability was necessary. The solution was four leveling jacks with wheels and swivel casters.

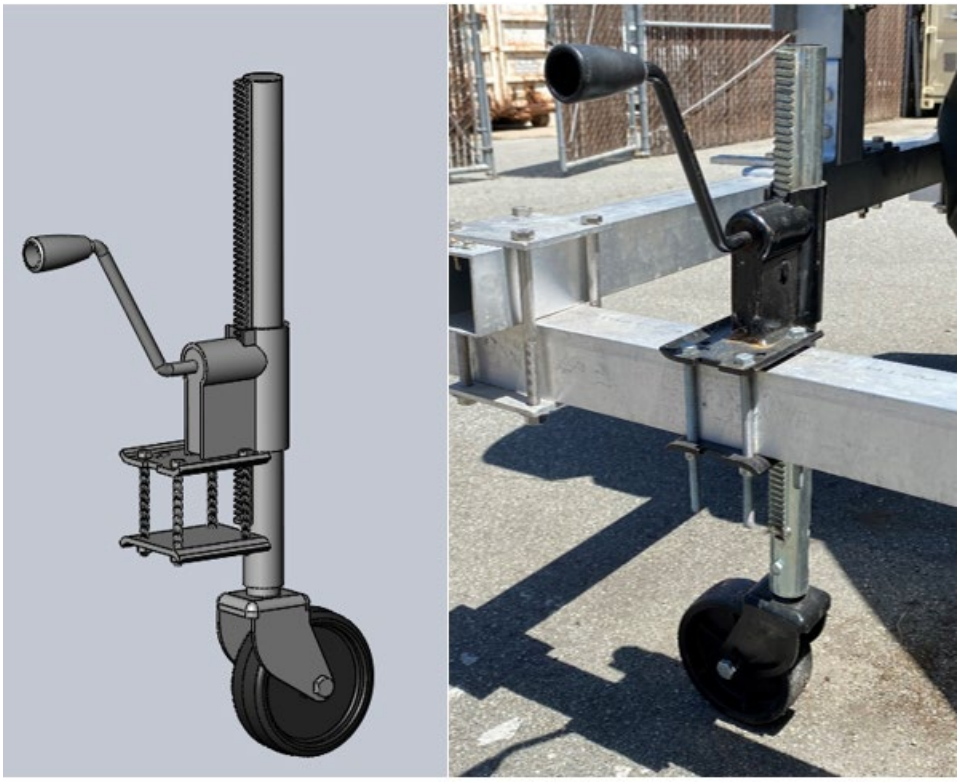

Figure 41. Solidworks model and the actual mounted leveling jack

Two of the leveling jacks were mounting in between the two flanges on the throttle casing and the other two were mounted forward of the center of mass, toward the inlet of the bell mouth. This prevented the whole assembly from being susceptible to tipping, as the center of mass fell in the middle of the four leveling jacks. The entire Solidworks assembly showing the locations of the leveling jacks and the actual manufactured assembly mounted on the front of the TCR are shown in Figures 42 and 43, respectively.

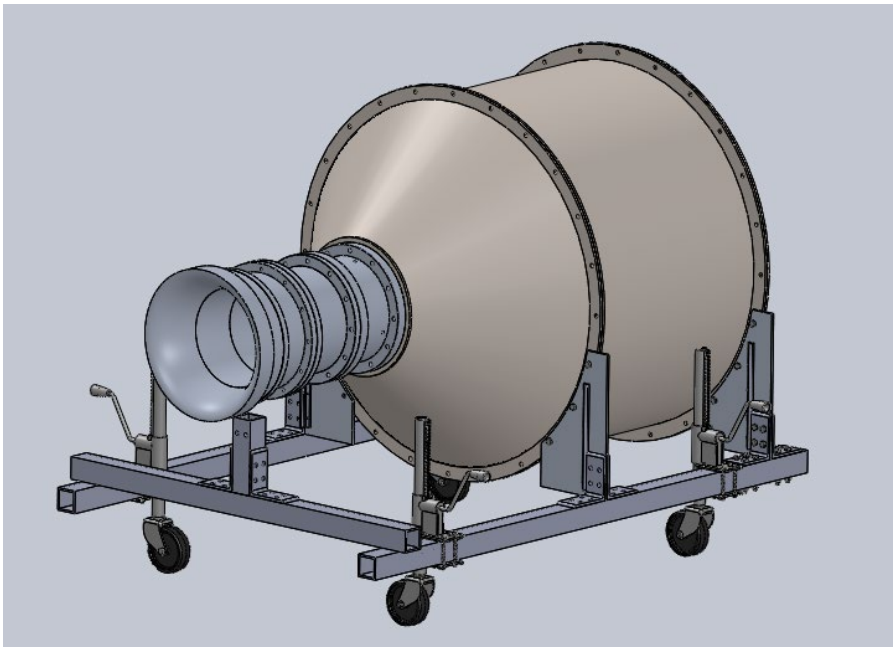

Figure 42. Solidworks model of full support structure attached to throttle casing and bell mouth

Figure 43. Manufactured support structure attached to the throttle casing and bell mouth

THIS PAGE INTENTIONALLY LEFT BLANK

VI. EXPERIMENTAL DATA AND CALCULATIONS

A. PROBE MOUNTING AND ORIENTATION

The flange to which the rake probe is mounted had 12 mounting bolts evenly spaced about the circumference making the angular difference between bolts 30°. The rake probe could be mounted at 30° increments, allowing tests to be conducted in order to check the axis-symmetry of the flow. The orientation of the bolts did not allow for exactly vertical mounting of the rake probe, but it could be mounted 15° on either side of the vertical. The initial mounting position was 15° clockwise from the vertical when looking into the bell mouth inlet from the front. The rake probe in this initial position is shown in Figure 44.

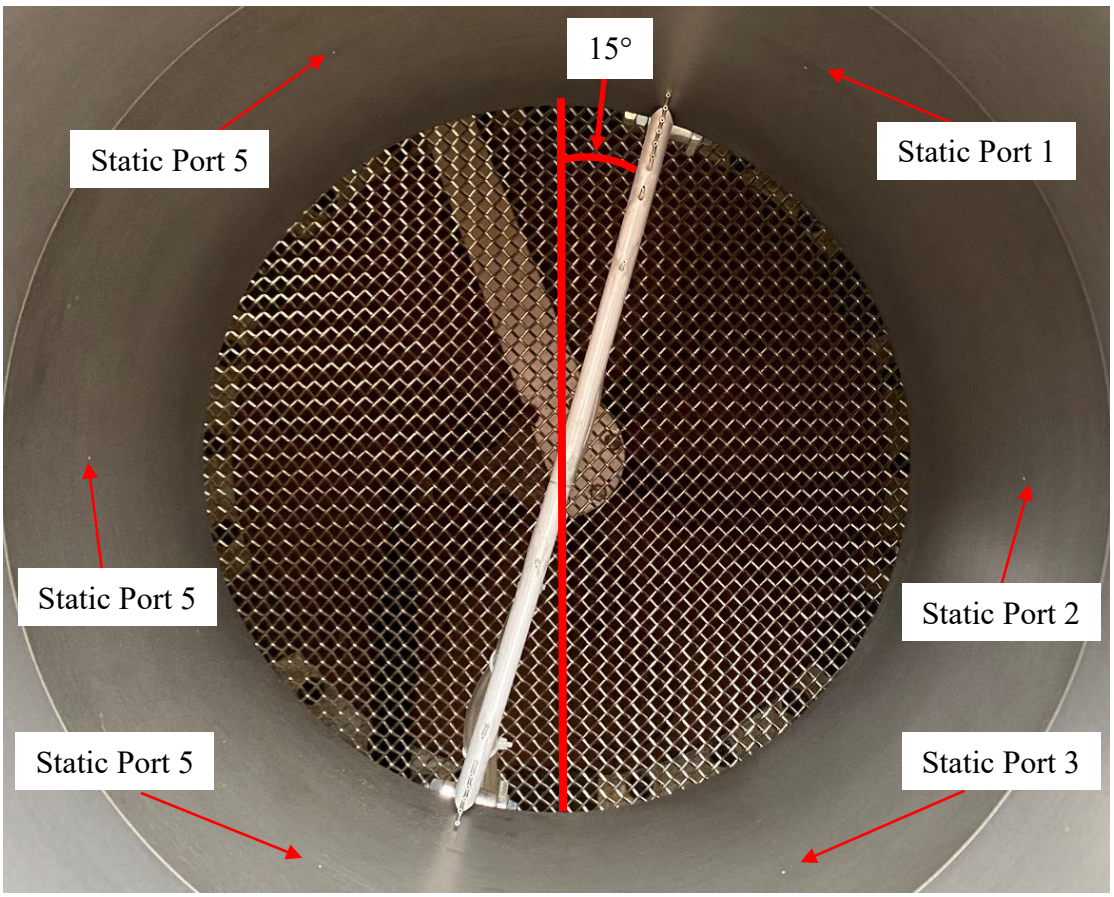

Figure 44. Initial orientation of the rake probe, 15° from the vertical

In the post processing of data, this initial position will be referred to as 0°, and any other orientations will be referred to by their relative angle to this initial position.

B. CALCULATIONS

The ultimate desire of this project was to calculate the discharge coefficient of the bell mouth inlet, which relates the actual mass flow rate to the ideal mass flow rate. The post processing of the raw data collected from the TCR includes calculating both of these mass flow rates. The ideal mass flow rate is relatively straight-forward to calculate and involves minimal instrumentation. This is why an accurate calculation of the discharge coefficient is so important: so that more complicated instrumentation to measure mass flow rate can be done away with and the ideal mass flow can be calculated and then converted to the real mass flow rate via the discharge coefficient.

The ideal mass flow rate through the bell mouth inlet is calculated using the static pressure at the inner wall of the bell mouth, the total pressure measured outside the flow, and the total temperature also measured outside the flow. The experimental mass flow, however, involves more complicated instrumentation to accurately measure the profile of the velocity across the cross section of the bell mouth. The ideal mass flow rate assumes this profile is uniform across the entire cross section, but it cannot be so due to the boundary layer. In order to approximate the velocity profile most accurately, the velocity and density are calculated at many discrete points in the flow through pressures measured with the rake probe. These velocities and respective densities were used to interpolate values across the whole radius of the bell mouth and then integrated over the cross-sectional area of the inlet, giving mass flow rate. The design of the rake probe previously discussed provided discrete data points at locations that would make the interpolation as accurate as possible.

The interpolation and integration of the velocity and density profiles were done in multiple ways. The least sophisticated and most broadly applicable method was to interpolate the profile using straight lines between the data points. Integrating this interpolated profile would result in a trapezoidal integration. This is simple to do in MATLAB, but has a relatively large uncertainty. The velocity profile is concave down, which means the trapezoidal integration scheme will always underestimate the mass flow

rate. The uncertainty with which the trapezoidal scheme underestimates the integral was calculated and can be used to adjust the mass flow rate calculated with this scheme.

The other way in which to interpolate and integrate the profiles is by fitting a curve to the data that smoothly connects the data points. First, a spline fit was attempted, but it performed poorly at preserving the approximate shape of the velocity profile. The MATLAB pchip (piecewise cubic Hermite interpolating polynomial) function was found to approximate the profile more accurately. This function generates a curve determined by shape-preserving piecewise cubic interpolation of the data provided to the function [7]. A plot comparing the trapezoidal and pchip interpolated profiles using the port side probes is shown in Figure 45.

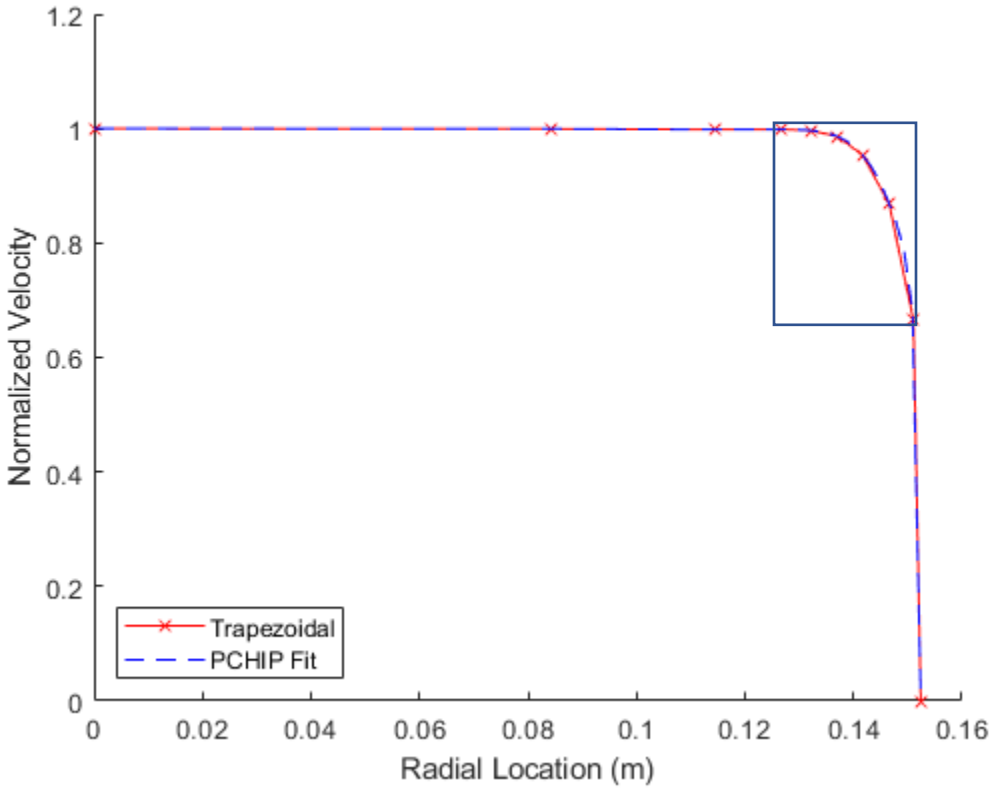

Figure 45. Trapezoidal and pchip interpolation schemes

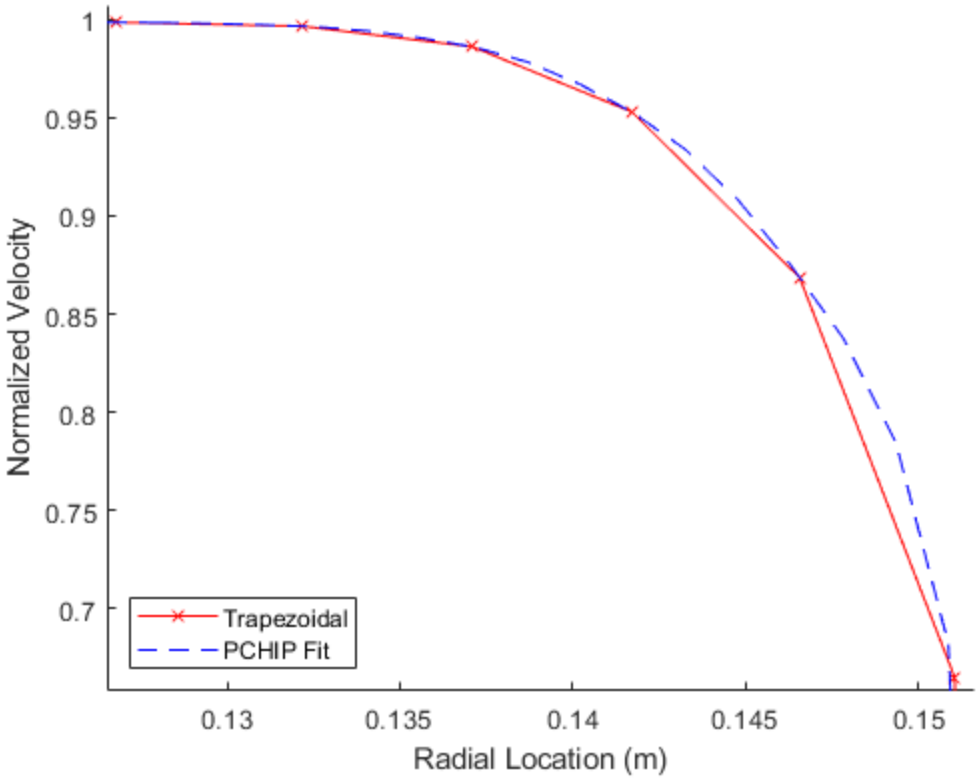

Figure 46. Closer view of the difference between the two interpolations

A plot showing discrete data from the entire rake probe (port and starboard side overlapped) with the pchip interpolated profile is shown in Figure 47. This interpolated profile is integrated to determine the mass flow rate using the entire rake probe. The smoothness of the data demonstrates the symmetric nature of the flow, as the data points were measured on opposite sides of the bell mouth.

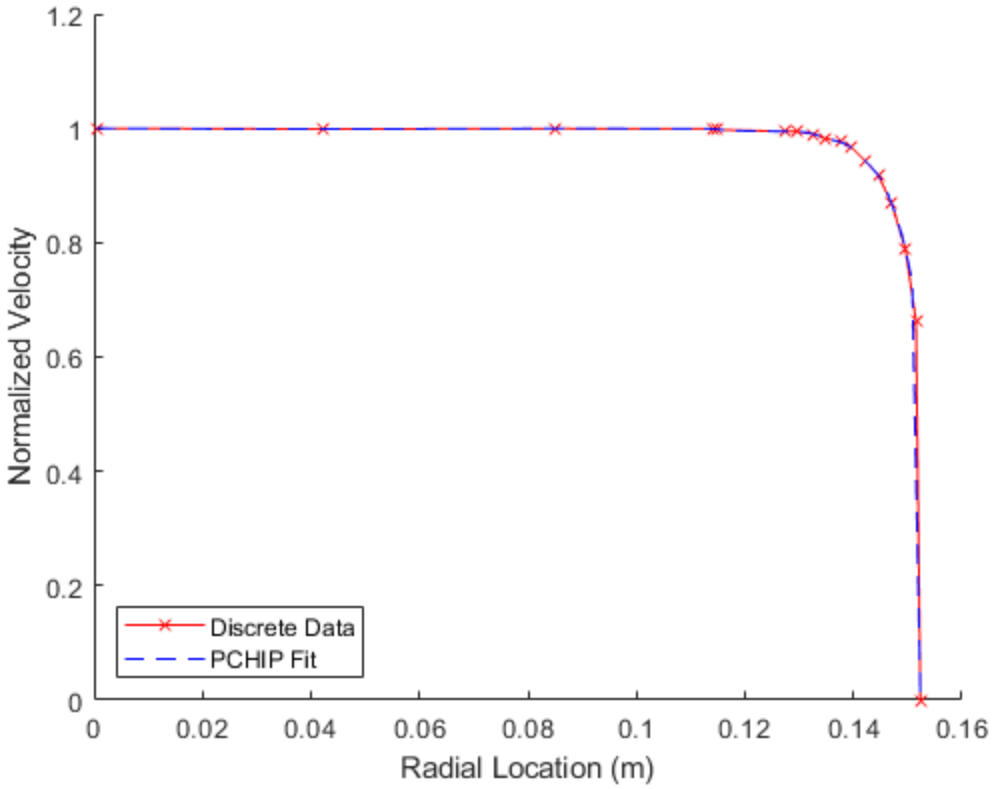

Figure 47. Total rake probe data with pchip fit interpolated profile.

C. RESULTS

Data was collected from the TCR at one second intervals over a variety of flow conditions. The post processing of the raw data in MATLAB involved calculating mass flow rate, Reynolds number, and discharge coefficient for each instance recorded. This allowed for an accurate representation of how the flow varies throughout the runs and can help identify any trends. From the values calculated for each second that data was collected, appropriate averages could be calculated to determine what the most appropriate discharge coefficient would be to use in further experimentation. The different flow conditions at which data was collected resulted in varying Reynolds number of the flow. Data was taken at 70% and 85% of the maximum rotational speed, and at throttle positions of approximately 0, 5, and 7. The discharge coefficient fluctuates through the run, but the Reynolds number for each run remains more constant. In this way, each run can be identified on a plot of all the data points collected. Data used in the calculations were

collected on five different days, at the two speeds, and from approximate mass flow rates of 4.5 kg/s to 8.5 kg/s with four steps in between.

The mass flow rate and discharge coefficient were calculated using the port probes, starboard probes and the total rake probe. This was done so that if any factors made the flow significantly non-axisymmetric, those trends could be identified. Assuming the flow is axisymmetric, the total rake probe would be the most accurate measurement because there are more probes spread across the cross section of the inlet to provide measurements at closer intervals. The port and starboard sides attempt to approximate what should be the same flow profile, but the differences between the two sides mean that their approximations will be slightly different. The data from all of the collected runs is shown in Figures 48–50 for the total rake probe, port side alone, and starboard side alone, respectively.

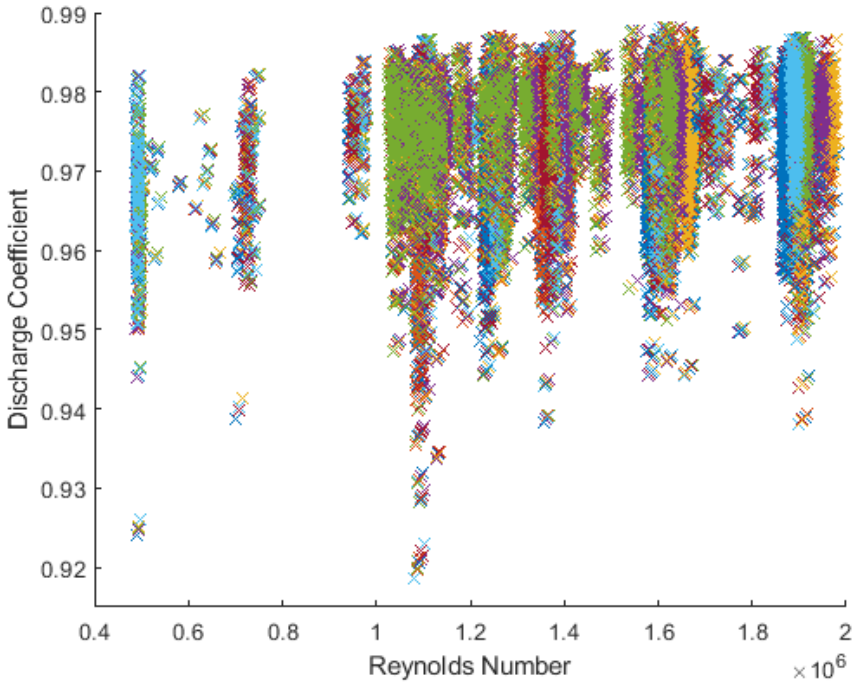

Figure 48. Total rake probe discharge coefficient as a function of Reynold's number

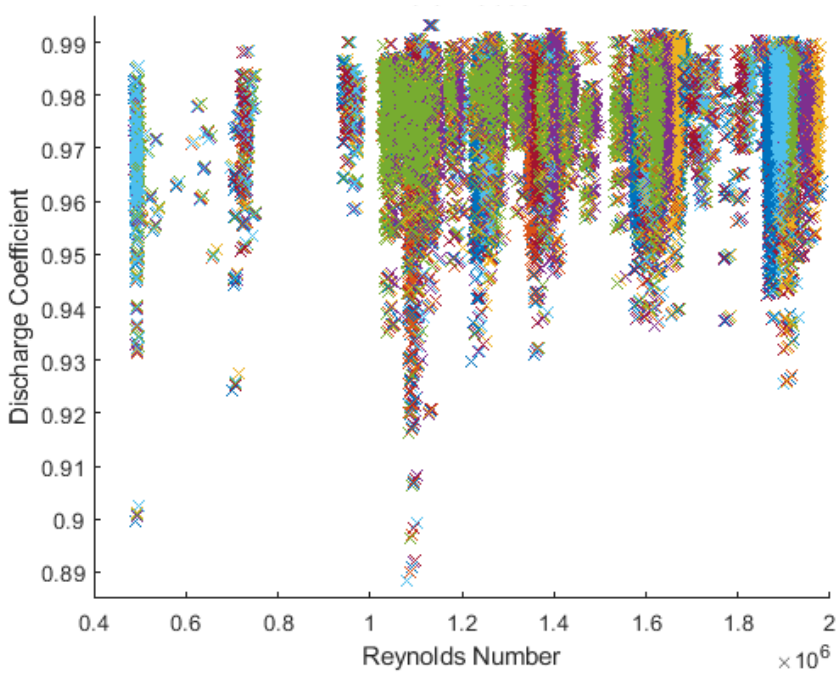

Figure 49. Port side of rake probe discharge coefficient as a function of Reynold's number

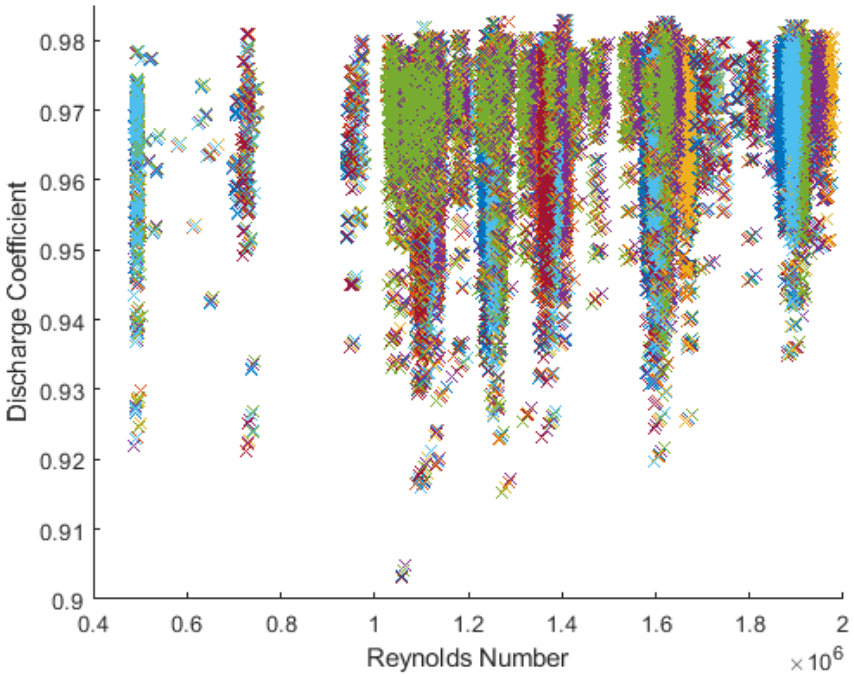

Figure 50. Starboard side of rake probe discharge coefficient as a function of Reynold's number

Though the discharge coefficient varies during each run, there does not seem to be a strong correlation between Reynold's number and discharge coefficient. This is important because it allows one single discharge coefficient to be used in the data acquisition system for its calculations for all flow conditions, rather than having to vary the discharge coefficient for different flow conditions based on the Reynold's number at that flow condition.

Due to each run having its own set of data independent of the others, an arithmetic mean was calculated for each run. The means from each run from the total rake probe, port side, and starboard side were then compiled onto three respective plots and the average of those averages were calculated. The scatter plots of the average discharge coefficient and Reynold's number from each run are shown in Figures 51–53.

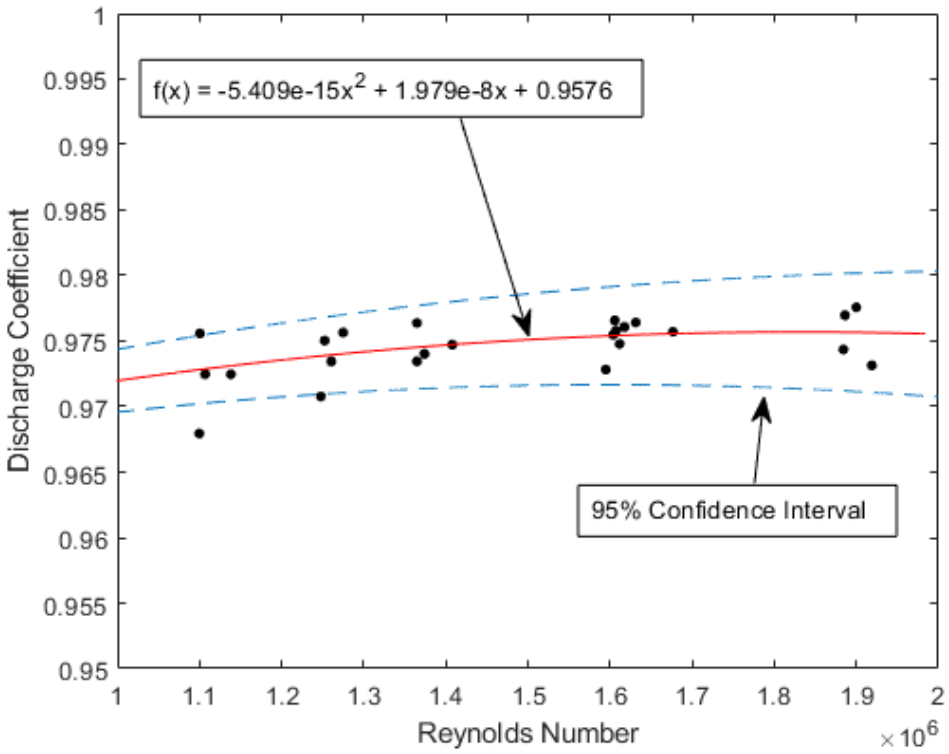

Figure 51. Average discharge coefficient from each run using the total rake probe.

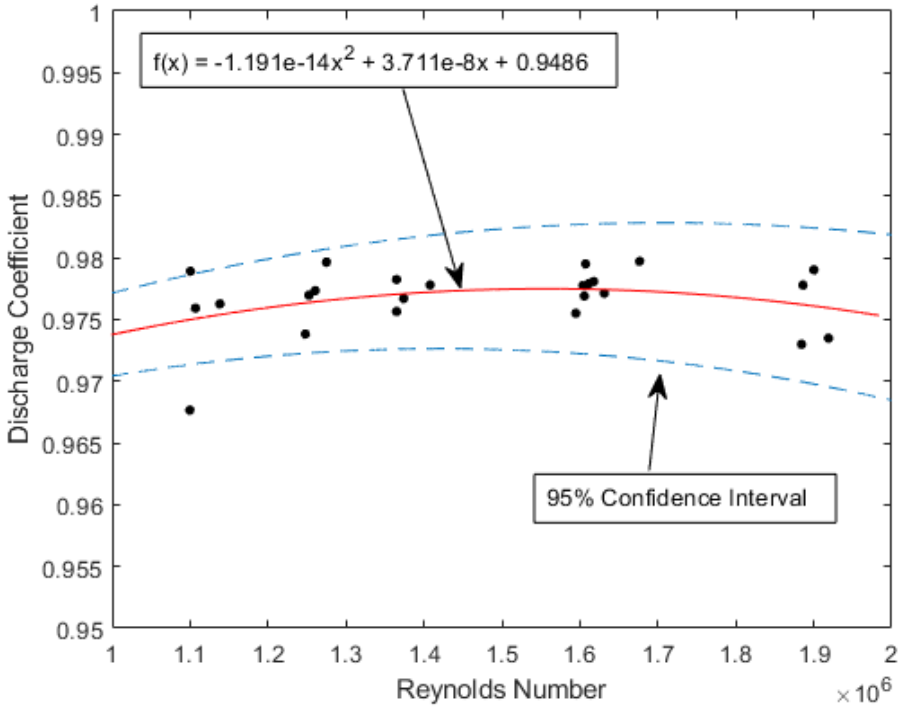

Figure 52. Average discharge coefficient from each run using the port side alone.

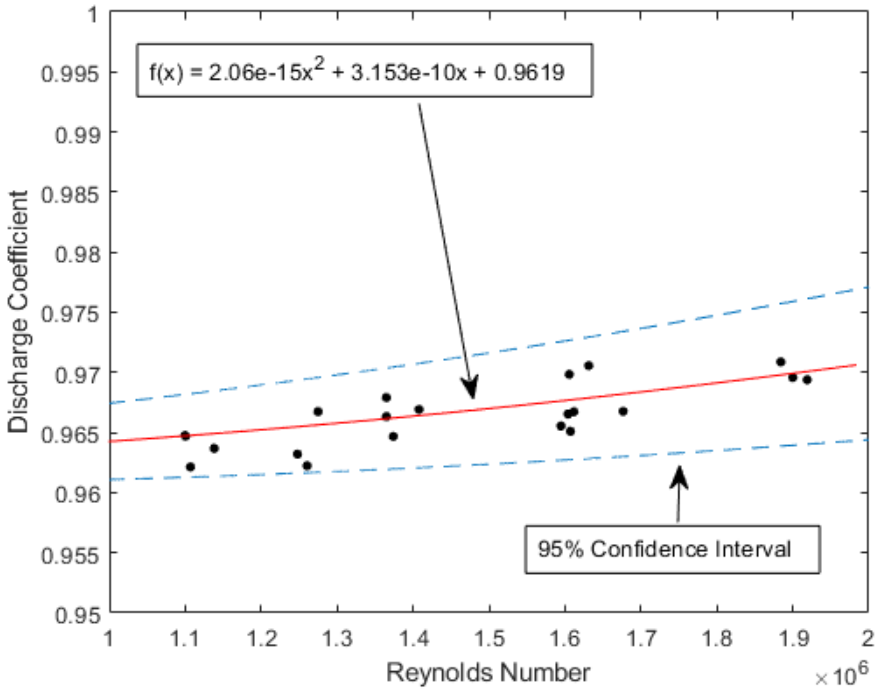

Figure 53. Average discharge coefficient from each run using the starboard side alone.

The starboard side alone seems to show a correlation between discharge coefficient and Reynold's number, but the port side alone and the total rake probe showed nearly no correlation. The starboard side alone also seems to approximate the discharge coefficient as lower than the total rake probe and the port side alone approximate the discharge coefficient above the total rake probe. The average from each of these plots are tabulated in Table 8.

Table 8. Average discharge coefficients

	Discharge Coefficient
Port Side	0.9763 ± 0.0177
Starboard Side	0.9669 ± 0.0169
Total Rake Probe	0.9745 ± 0.0128
CFD	0.9647

VII. CONCLUSION

A. SUMMARY

This study sought to attain an accurate means of measuring the mass flow rate through the inlet of the TCR. A CFD analysis of the inlet of the TCR provided an approximation of the flow profile in the bell mouth, where mass flow measurements were taken. The bell mouth inlet was implemented on the TCR, providing desirable flow conditions for mass flow measurements. The approximation from the CFD analysis drove the design of a rake probe that was designed to be mounted in the throat of the bell mouth and experimentally measure the velocity profile. The actual velocity profile of the flow in the bell mouth was integrated over the cross section of the inlet to determine the actual mass flow rate. This experimental mass flow rate was used to determine the discharge coefficient of the bell mouth, which was calculated to be 0.9745 ± 0.0128. This value compared well to the CFD calculations as well as previous studies that calibrated other bell mouths.

B. FUTURE WORK

Future work should involve developing a higher fidelity CFD analysis. The CFD analysis in this study simplified the geometry in some ways. For use as a scoping tool that led to the design of a rake probe, the geometry was sufficiently accurate. However, for the CFD to be used for any detailed analysis itself, the smaller details of the design would have some impact. Additionally, this CFD model investigates air upstream of the throttle. Further investigations should integrate this design into a model of the entire TCR, including downstream ducting, which contains flow straightening screens.

More future work should involve the implementation of a new rake probe that will be mounted just upstream of the compressor fan. This new rake probe will provide a detailed understanding of the flow profile as it reaches the compressor. Highly accurate data about the flow profile when it reaches the compressor is extremely valuable when it comes to monitoring compressor performance and stall prediction. The new rake probe uses the same principles as the rake probe in the bell mouth, but will have a difference

design. Rather than one rake across the middle of the flow, this rake will have three radial components that meet at the flow center and are separated by 120°. The new rake probe is shown in Figure 54.

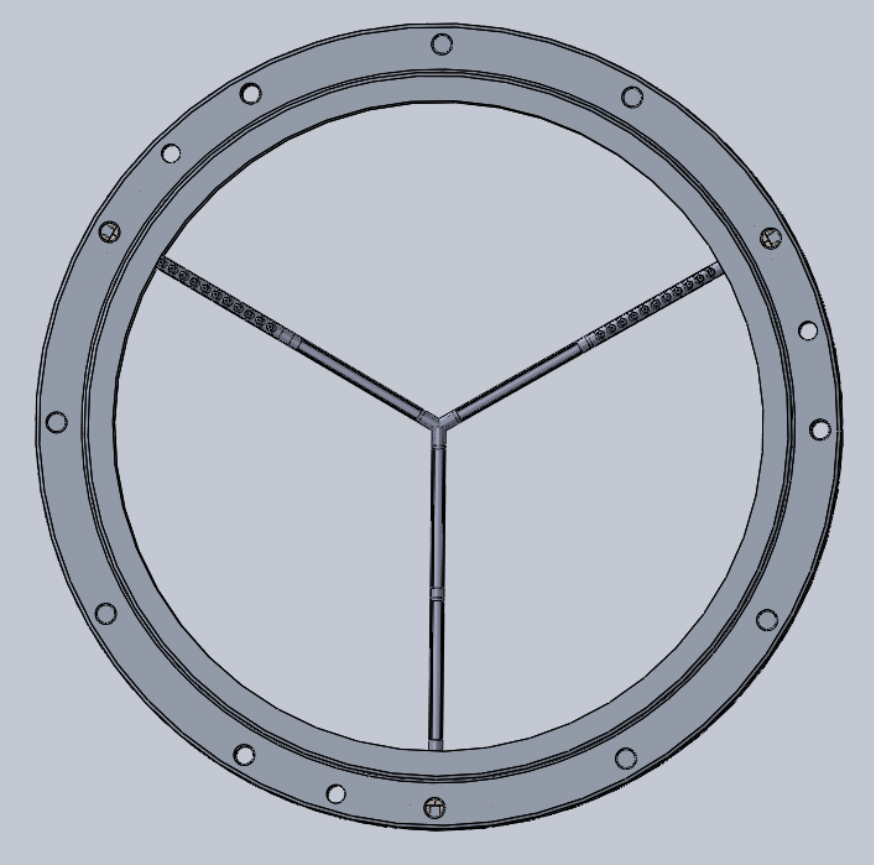

Figure 54. New rake probe viewed from upstream

One of the individual arms of the rake probe is shown in Figure 55. The radial position of the pitot tubes shown in Figure 55 will be adjusted to optimize the design so that it better measures the flow profile. This process is similar to that conducted in this thesis.

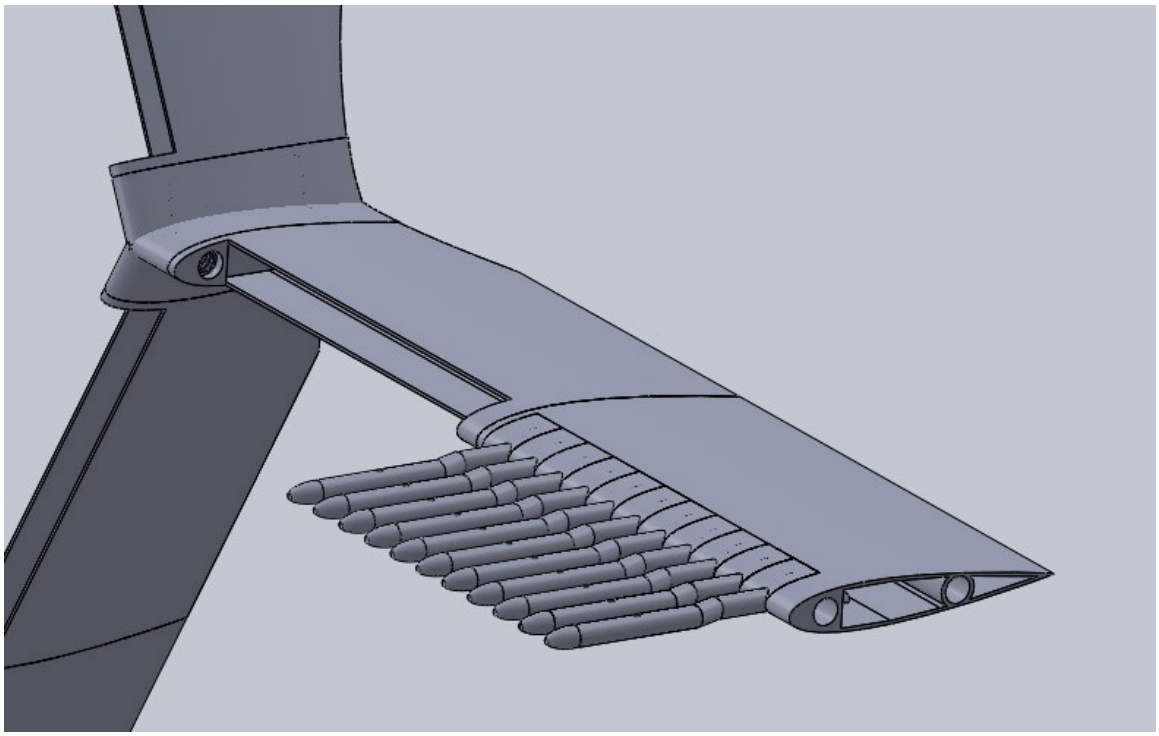

Figure 55. One arm of the new rake probe

THIS PAGE INTENTIONALLY LEFT BLANK

APPENDIX

Travis Grant

Post Processing of Rake Probe data

```
clear;
clc;
close all;
```

Constants

```
rad = 0.0254*(11.995/2);     % Inner radius of bell mouth inlet in meters
A = pi*rad*rad;              % Cross sectional area of bell mouth inlet m^2
```

Probe Locations

```
probes = [-5.907,-5.7085,-5.5145,-5.318,-5.1185,-4.517,-
1.675,0,3.322,4.5035,4.9925,5.2035,5.3975,5.579,5.7705,5.947];

starboard_probes = 0.0254.*(sort(-probes(1:8))); % probes 9-16 from center to wall,
meters
starboard_probes(9) = rad;
```

```
port_probes = 0.0254.*probes(8:16);  % probes 1-8 from center to wall, meters
port_probes(10) = rad;
```

```
probes_all = 0.0254.*(sort(abs(probes)));  % All probes in meters
probes_all(17) = rad;
```

Load Data

```
tic
[data_85pct_16apr,txt,raw] = xlsread('85pct04162021.xlsx');
toc
```

Preallocating

```
endloop = 1526;  % number of data points in data file

m_dot_all = zeros(endloop,6);
m_dot_port = zeros(endloop,6);
```

```
m_dot_starboard = zeros(endloop,6);
m_dot_ideal = zeros(endloop,6);

rho_ideal = zeros(endloop,6);
v_ideal = zeros(endloop,6);

C_d_all = zeros(endloop,6);
C_d_port = zeros(endloop,6);
C_d_starboard = zeros(endloop,6);

mu_interp = zeros(endloop,6);
```

Loop

```
for i = 1:endloop    % All lines of data from data file
    for j = 120:125  % Static Ports 1-6
```

```
        gamma = data_70pct_02apr(i,171);  % ratio of specific heats
         Cp = data_70pct_02apr(i,172);     % isobaric specific heat
         R = data_70pct_02apr(i,173);      % gas constant for air

         Ps = data_70pct_02apr(i,j);       % static ports: 120:125


         % Total temperature measurements are redundant, average used
         T_t1 = data_70pct_02apr(i,17);  % Total temperature 1
         T_t2 = data_70pct_02apr(i,18);  % Total temperature 2
         T_t = (T_t1+T_t2)/2;            % Average Total temperature

         % Total pressure measurements are redundant, average used
         P_t1 = data_70pct_02apr(i,126); % Total pressure 1
         P_t2 = data_70pct_02apr(i,127); % Total pressure 2
         P_t = (P_t1+P_t2)/2;            % Average total pressure
```

Ideal Calculations

Ideal density

```
       rho_ideal(i,(j-119)) = (P_t./(R*T_t)).*(Ps./P_t).^(1./gamma);
         % Ideal Velocity
         v_ideal(i,(j-119)) = sqrt(abs(1-(Ps./P_t).^((gamma-
1)./gamma))).*sqrt(2.*Cp.*T_t);
         % Ideal Mass Flow rate
         m_dot_ideal = rho_ideal.*A.*v_ideal;
         %%%%%%%%%%%%%%%%%%%%%%%%%%%%%%%%%%%%%%%%%%%%%%%%%%%%%%%%%%%%%%%%%%%%


         %%%%%%%%%%%%%%%%%%%%%%%%%%%%%%%%%%%%%%%%%%%%%%%%%%%%%%%%%%%%%%%%%%%%
         % Total Pressure measured at each rake probe pitot tube (1-16)
         P1 = data_70pct_02apr(i,128);
         P2 = data_70pct_02apr(i,129);
```

```
        P3 = data_70pct_02apr(i,138);
        P4 = data_70pct_02apr(i,139);
        P5 = data_70pct_02apr(i,140);
        P6 = data_70pct_02apr(i,141);
        P7 = data_70pct_02apr(i,142);
        P8 = data_70pct_02apr(i,143);
        P9 = data_70pct_02apr(i,144);
        P10 = data_70pct_02apr(i,145);
        P11 = data_70pct_02apr(i,146);
        P12 = data_70pct_02apr(i,147);
        P13 = data_70pct_02apr(i,148);
        P14 = data_70pct_02apr(i,149);
        P15 = data_70pct_02apr(i,130);
        P16 = data_70pct_02apr(i,131);

        press_all = [P9,P10,P8,P7,P11,P6,P12,P5,P13,P4,P14,P3,P15,P2,P16,P1];
        press_starboard = [P9,P10,P11,P12,P13,P14,P15,P16];
        press_port = [P9,P8,P7,P6,P5,P4,P3,P2,P1];

        % Calculations will include the pressure at the wall, which is the
        % static pressure
        press_port(:,10) = Ps;
        press_starboard(:,9) = Ps;
        press_all(:,17) = Ps;
        %%%%%%%%%%%%%%%%%%%%%%%%%%%%%%%%%%%%%%%%%%%%%%%%%%%%%%%%%%%%%%%%%%%%%%%

        %%%%%%%%%%%%%%%%%%%%%%%%%%%%%%%%%%%%%%%%%%%%%%%%%%%%%%%%%%%%%%%%%%%%%%%
        % Rake Probe Calculations
        % Velocity at each probe location
        v_port = sqrt(abs(1-(Ps./press_port).^((gamma-1)./gamma))).*sqrt(2*Cp.*T_t);
        v_starboard = sqrt(abs(1-(Ps./press_starboard).^((gamma-
1)./gamma))).*sqrt(2*Cp.*T_t);
        v_all = sqrt(abs(1-(Ps./press_all).^((gamma-1)./gamma))).*sqrt(2*Cp.*T_t);

        % Density at each probe location
        rho_port = (press_port./(R*T_t)).*(Ps./press_port).^(1/gamma);
        rho_starboard = (press_starboard./(R*T_t)).*(Ps./press_starboard).^(1/gamma);
        rho_all = (press_all./(R*T_t)).*(Ps./press_all).^(1/gamma);

        % PCHIP spline based on density, velocity and location of probes
        port_spl = pchip(port_probes,(rho_port.*v_port));
        starboard_spl = pchip(starboard_probes,(rho_starboard.*v_starboard));
        all_spl = pchip(probes_all,(rho_all.*v_all));
        %%%%%%%%%%%%%%%%%%%%%%%%%%%%%%%%%%%%%%%%%%%%%%%%%%%%%%%%%%%%%%%%%%%%%%%

        %%%%%%%%%%%%%%%%%%%%%%%%%%%%%%%%%%%%%%%%%%%%%%%%%%%%%%%%%%%%%%%%%%%%%%%
        % Integrations for mass flow rates
        m_dot_all(i,(j-119)) = 2*pi*integral(@(x) x.*ppval(all_spl,x),0,rad);
        m_dot_starboard(i,(j-119)) = 2*pi*integral(@(x) x.*ppval(starboard_spl,x),0,rad);
        m_dot_port(i,(j-119)) = 2*pi*integral(@(x) x.*ppval(port_spl,x),0,rad);
        %%%%%%%%%%%%%%%%%%%%%%%%%%%%%%%%%%%%%%%%%%%%%%%%%%%%%%%%%%%%%%%%%%%%%%%
```

Reynolds No. Calcs

```
% Interpolation of Dynamic Viscosity for each data point
 mu_o = 1.716*(10^-5); % standard Dynamic Viscositykg/m-s
 T_o = 273.15;  % standard temperature K
 S = 110.4; % K
 T_first = data_70pct_02apr(1,17);
 T_last = data_70pct_02apr(endloop,17);

 mu_first = mu_o*((T_first/T_o)^1.5)*((T_o+S)/(T_first+S));
 mu_last = mu_o*((T_last/T_o)^1.5)*((T_o+S)/(T_last+S));

 mu_diff = (mu_last-mu_first)/endloop;
 mu_interp(i,(j-119)) = mu_first+(i*mu_diff); % interpolated mu

 D = 2*rad;  % bell mouth diameter in meters
```

Discharge Coefficients

```
C_d_port = m_dot_port./m_dot_ideal;
C_d_starboard = m_dot_starboard./m_dot_ideal;
C_d_all = m_dot_all./m_dot_ideal;
```

Reynold's Number

Calculated for each data point

```
Re = rho_ideal.*v_ideal.*D./mu_interp;
```

CFD Cd calcs

```
[cfd_data,txt,raw] = xlsread('CFD Cd 60deg Calcs.xlsx');

P_amb = cfd_data(1,6)+101300;  % total pressure
P_stat = cfd_data(7,6)+101300; % static pressure
T_amb = cfd_data(1,8);         % total temperature
rho_amb = cfd_data(1,4);       % density at ambient
Cp_cfd = cfd_data(1,7);        % isobaric specific heat
mu_cfd = cfd_data(1,5);        % dynamic viscosity

rho_cfd = rho_amb.*(P_stat./P_amb).^(1./gamma);  % adjusted density
v_cfd = sqrt(abs(1-(P_stat./P_amb).^((gamma-1)./gamma))).*sqrt(2.*Cp_cfd.*T_amb);
m_dot_ideal_cfd = rho_cfd.*A.*v_cfd;  % ideal mass flow rate
m_dot_actual_cfd = cfd_data(11,3);    % mass flow rate given from CFX
Cd_cfd = m_dot_actual_cfd/m_dot_ideal_cfd;  % CFD Discharge coefficient

Re_cfd = rho_cfd.*v_cfd.*D./mu_cfd;   % CFD Reynold's Number
```

Published with MATLAB® R2020b

LIST OF REFERENCES

[1] Smith, S.C., 1985, "Airflow Calibration of Bellmouth Inlet for Measurement of Compressor Airflow in Turbine-Powered Propulsion Simulators," NASA Technical Memorandum No. NASA-TM-84399.

[2] Polak, T. and Pande, C., 1999, "Fluid Flow Measurement," Engineering Measurements, John Wiley & Sons, LTD, Chichester, UK

[3] Ito, H., Watanabe, Y., Shoji, Y., 1984, "A Long Radius Inlet Nozzle for Flow Measurement," J. Phys. E: Sci. Instrum., 18, pp. 88–91.

[4] Wallen, J.M., 2020, "Inlet Mass Flow Modeling and Measurement Through a Transonic Axial Compressor Fan." M.S. thesis, Naval Postgraduate School, Monterey, CA, USA.

[5] The American Society of Mechanical Engineers, 2011, "Measurement of Gas Flow by Bellmouth Inlet Flowmeters," MFC-26. New York, New York, USA.

[6] Pankhurst, R.C. and Holder, D.W., 1952, Wind-Tunnel Technique, Sir Isaac Pitman & Sons, LTD, London, UK.

[7] "Piecewise Cubic Hermite Interpolating Polynomial (PCHIP)," MathWorks Help Center, accessed April 15, 2021, https://www.mathworks.com/help/matlab/ref/pchip.html.

THIS PAGE INTENTIONALLY LEFT BLANK

INITIAL DISTRIBUTION LIST

1. Defense Technical Information Center
   Ft. Belvoir, Virginia

2. Dudley Knox Library
   Naval Postgraduate School
   Monterey, California